

The Evolution of the Multiplicity of Embedded Protostars I: Sample Properties and Binary Detections¹

Michael S. Connelley¹, Bo Reipurth², and Alan T. Tokunaga³

ABSTRACT

We present the observational results of a near-infrared survey of a large sample of Class I protostars designed to determine the Class I binary separation distribution from ~ 100 AU to ~ 5000 AU. We have selected targets from a new sample of 267 nearby candidate Class I objects. This sample is well understood, consists of mostly Class I young stellar objects (YSOs) within 1 kpc, has targets selected from the whole sky, and is not biased by previous studies of star formation. We have observed 189 Class I YSOs north of $\delta = -40^\circ$ at H, K and L'-bands, with a median angular resolution of $0''.33$ at L'. We determine our detection limit for close binary companions by observing artificial binaries. We choose a contrast limit and an outer detection limit to minimize contamination and to ensure that a candidate companion is gravitationally bound. Our survey uses observations at L' rather than K-band for the detection of binary companions since there is less scattered light and better seeing at L'. This paper presents the positions of our targets, the near-IR photometry of sources detected in our fields at L', as well as the observed properties of the 89 detected companions (73 of which are newly discovered). Although we have chosen contrast and separation limits to minimize contamination, we expect that there are ~ 6 stars identified as binary companions that are due to contamination. Finder charts at L' for each field are shown to facilitate future studies of these objects.

Subject headings: binaries: general, stars: formation, stars: statistics, infrared: stars

¹Michael.S.Connelley@nasa.gov, NASA Ames Research Center, MS 245-6, Moffett Field, CA 94035

²University of Hawai'i Institute for Astronomy, 640 N. Aohoku Pl., Hilo HI 96720

³University of Hawai'i Institute for Astronomy, 2680 Woodlawn Dr., Honolulu, HI 96822

¹The Infrared Telescope Facility is operated by the University of Hawaii under Cooperative Agreement no. NCC 5-538 with the National Aeronautics and Space Administration, Science Mission Directorate, Planetary Astronomy Program. The United Kingdom Infrared Telescope is operated by the Joint Astronomy Centre on behalf of the Science and Technology Facilities Council of the U.K. Based in part on data collected at Subaru Telescope, which is operated by the National Astronomical Observatory of Japan.

1. Introduction

Ever since it was demonstrated that there must be physically bound pairs of stars and star clusters (Mitchell 1767), the question of binary star formation has been an unsolved problem in astronomy. Duquennoy & Mayor (1991) reported that the solar-type main sequence binary frequency² is $50\% \pm 5.5\%$ for stars with periods from less than a day to over 10 million years without completeness correction, and 61% after completeness correction. Based on the statistics of the main-sequence binary population, Larson (2001) concluded that “stars seldom if ever form in isolation”.

The binary frequency of T Tauri stars has also been carefully studied because they are young, there are a large number of them, and they are optically visible. Reipurth & Zinnecker (1993) conducted an optical survey of 238 southern pre-main sequence stars and found a binary frequency of $16\% \pm 3\%$ over the range of projected separations from 150 to 1800 AU. More recently, Mathieu et al. (2000) and Patience et al. (2002) tabulated the results of multiplicity surveys among pre-main sequence stars. Overall, T Tauri stars are found to have roughly twice the binary frequency compared to main sequence solar type stars over the separation ranges covered by these studies.

Duchêne et al. (2004) and Haisch et al. (2004) have published results from searches for embedded binary YSOs in nearby star forming regions. Duchêne et al. (2004) found a binary frequency of $\sim 26\% \pm 8\%$ in the separation range from 110 AU to 1400 AU in a survey of 63 flat spectrum and Class I YSOs in the Taurus and Ophiuchus clouds. Haisch et al. (2004) observed a similar sample of 76 YSOs in the Perseus, Taurus, Chamaeleon, Ophiuchus, and Serpens clouds, finding a binary frequency of $18\% \pm 4\%$ in the separation range from 300 AU to 2000 AU. Combining both results, Duchêne et al. (2007) found a total of 19 companions to 119 stars, yielding a binary frequency of $16\% \pm 4\%$ from 300 to 1400 AU. This is roughly twice the binary frequency of main sequence stars over the same separation range, and is consistent with the binary frequency of T Tauri stars.

We have performed a major study of the binarity of Class I sources, which we present in this and a companion paper (Connelley et al. 2008, hereafter Paper II). New observations were required to investigate a larger sample spread over a wider range of star forming regions at higher angular resolution than previous studies. The goal of this paper is to present the sample of Class I YSOs we observed (section 2) and our observational results (section 3). We discuss how we identified binaries and minimized contamination through a choice of contrast and separation limits (section 4). We also include the properties of the binary companions

²The binary frequency is the total number of companion stars divided by the number of systems.

that we found, including binary systems with strong color differences (section 5) that are analogues to infrared companions to T Tauri stars. In Paper II we present the Class I binary separation distribution using the data presented here. That paper also includes comparisons of the Class I binary separation distribution with the results of previous studies of Class I YSOs and other pre-main sequence stars, the evolution of the binary separation distribution within the Class I phase, and the dependence of the Class I binary frequency on the star forming environment.

2. Sample Properties

We used a new sample of nearby mostly Class I YSOs described in Connelley et al. (2007). Briefly summarized, the sample was selected based on IRAS colors, coincidence with nearby dark clouds, and coincidence with a red ($H-K \gtrsim 1$) 2MASS source. Distance estimates, usually to the cloud hosting the protostar, were taken from the literature and are listed in Table 1, along with the source of the distance estimate. The distance distribution (Figure 1) shows that most objects are within 1 kpc, with a median distance of 470 pc. We do not have distance estimates to all of the targets in our sample, however several targets without distance estimates appear to be associated with well known clouds. The spectral index distribution (Figure 2) shows that the majority of our targets have a spectral index (Lada 1991) greater than 0, and thus the majority are Class I objects. However, there are a few known T Tauri stars in our sample. For example, FS Tau A was observed since it is a companion to FS Tau B, which is deeply embedded. The sample’s spectral index distribution has a median value of +0.79 and a mean value of +0.91. These spectral indices were derived using only IRAS fluxes from the Faint Source Catalog if the target is included in that catalog, or the Point Source Catalog if not. We used flux measurements from 12 μm to 100 μm , unless the 12 μm measurement is an upper limit, in which case the spectral index was calculated from 25 μm to 100 μm . Several IRAS sources have more than one near-IR counterpart in the IRAS beam, thus higher angular resolution far-IR observations may yield different values for the spectral index. The bolometric luminosities of all sources were calculated as described in Connelley et al. (2007). The dearth of sources with $L_{bol} > 100 L_{\odot}$ suggests that relatively few of the stars in the sample are high mass stars. This is expected since Connelley et al. (2007) selected against sources associated with HII regions. Similarly, the dearth of sources with $L_{bol} < 0.5 L_{\odot}$ shows that it is unlikely that there are many proto-brown dwarfs in the sample.

A goal of the sample selection process was to choose sources across the entire sky, without bias towards well known star forming regions. Figure 3 shows the distribution of

targets in Galactic coordinates. The shaded area on the right is the part of the sky that is south of $\delta = -40^\circ$. Targets in this region do not rise above 2 airmasses from Mauna Kea and, aside from two exceptions, were not observed. Our targets are spread across all Galactic longitudes, with clumping in the Taurus/Auriga and Orion star forming regions. These two regions are both below the Galactic plane and near the Galactic anti-center. Figure 4 shows the arrangement of targets as seen from above the Galactic plane. The targets that are in our sample, including those too far south for us to observe, are listed in Table 1.

3. Observations

3.1. Target Selection

Not all of the targets in the sample were observed in the course of our study. Some of the objects in the sample are T Tauri stars, while others are Class 0 objects, or a filament or knot in a cloud. A few of the stars in our sample are examples of what have become known as “transitional” objects, i.e. objects between Class I and T Tauri stars with a spectral index near 0. These sources were observed as they satisfied our selection criteria and since the studies by Haisch et al. (2004) and Duchêne et al. (2004) include such objects. We did not attempt to observe the Class 0 objects since there is typically no flux in the near-IR. In some cases, MSX (Price et al. 2001) observations showed that the IRAS point source was a knot or a filament in a cloud, and not a true point source. Such sources have no near-IR counterpart and were not observed.

3.2. Observation Methods

Previous studies of the Class I binary frequency (Haisch et al. 2004 and Duchêne et al. 2004) searched for binary companions at K-band. We found that the seeing was better and more stable at L' than at K-band, and that reflection nebulae (which tend to have blue colors) are much less of a problem at L' . The bright sky background at L' also made it more difficult to see stars without an IR excess, reducing the effect of background star contamination. We therefore focused our search for binary companions on our L' observations and used the K-band and H-band observations for additional photometry.

Since we wanted to observe a large number of targets from H through L' , we chose telescope/instrument combinations that have this capability in one instrument, have good image quality, and have a suitable plate scale. We used the UH 2.2 m telescope with QUIRC (1024^2 HgCdTe 1-2.5 μm 3' FOV, Hodapp et al. 1996), the NASA IRTF with the SpeX

guider (512² InSb 1-5 μm 1' FOV, Rayner et al. 2003) and NSFCam2 (2048² Hawaii-2RG 1-5.5 μm 82'' FOV), UKIRT with UIST (1024² InSb 1-5 μm 1' FOV, Ramsay Howat et al. 2004), and Subaru Telescope with CIAO (1024² InSb 1-5 μm 22'' FOV, Murakawa et al. 2004) and IRCS (1024² InSb 1-5 μm 1' FOV, Tokunaga et al. 1998 and Kobayashi et al. 2000). Table 2 lists which telescopes were used on which nights. The majority of our observations used UKIRT and UIST, primarily due to the availability of observing time. Due to UKIRT's north declination limit of +60°, IRTF observations targeted sources north of this limit up to the north declination limit of IRTF (+70°). We used Subaru to observe targets north of this, targets for which we did not get good image quality with IRTF, and to observe targets with adaptive optics (AO).

Dithering was used for all observations in order to remove bad pixels and the detector flat field effects. A 3×3 dither pattern was typically used, the size of which was usually 5'' to 10'' and depended on the field of view of the instrument and the availability of guide stars. In the case of L' observations, coadds were used to increase the effective integration time per dither position to ~ 20 s to increase observing efficiency. Standard stars that have been observed by UKIRT through the MKO filter set (Simons & Tokunaga 2002, Tokunaga & Simons 2002) were selected from the UKIRT faint standard star list, and were observed for photometric calibration. Furthermore, the instruments we used have MKO filters, and thus all of our observations are in the MKO photometric system.

All data were reduced using the following procedure except in the case of the IRTF data, where the data were first divided by the product of the number of coadds and the number of non-destructive reads. A dark frame was made by averaging together 10 individual darks of the same exposure time as the science data. This dark was then subtracted from each target frame. To make the sky frame, each dark subtracted frame was scaled to have the same median value, then averaged together using a min-max rejection. The resulting sky frame was then normalized using the median value of the pixel counts. Each dark subtracted (non-scaled) target frame was divided by this normalized sky flat. The median sky value for each frame was subtracted from each frame to set the average background counts in each frame to 0. The images were then aligned and averaged together using an average sigma clipping rejection. In addition, images with better than average resolution were combined into a higher resolution image. This rejects images where the seeing was particularly poor or where there was a guiding error. Since most of the L' "sky" brightness is from the telescope, the procedure we used was not optimal for making a true L' flat field. However, the L' flats we used were effective for removing the detector's flat field response.

For this project, having the best angular resolution possible was critical. Particular attention was paid on maintaining the best focus possible. In the case of our IRTF observa-

tions with the SpeX guider, the image resolution was often limited by aberrations either in the telescope or in the instrument. Aberrations in UIST on UKIRT also occasionally limited our resolution at K, but rarely at L'. We used the 0''.06 plate scale in UIST in order to be able to use a longer exposure time at L' and to better sample the PSF. The resulting 1' FOV also allowed objects within 4500 AU of the target to be in the field of view for the closest targets. The angular resolution distributions at H, K, and L' are presented in Figure 5. The median FWHM was 0''.609 at H-band, 0''.543 at K-band, and 0''.335 at L'-band. The L'-band median FWHM includes our AO observations.

3.3. AO Observations

The selection of targets in nearby dark clouds naturally selected against nearby bright stars that could be used as AO guide stars. To find sources with a suitable visual guide star, we searched through the USNO-B1.0 catalog (Monet et al. 2003) for stars within 40'' of the near-IR source that are brighter than R or I=16. The objects that we observed with AO are presented in Table 3. To reduce the chance of reflection nebulosity interfering with our search for very close companions, we only observed sources with no resolved nebulosity in our seeing-limited L'-band data.

There are a number of cases where enough of the visible light from the YSO is able to escape the cloud to use the YSO itself as a guide star. This raises the possibility that the AO observed sub-sample is, on average, older and more evolved than the sample as a whole. We used the Kolmogorov-Smirnov test to determine if the AO observed sub-sample is different from the whole sample based on the spectral index and bolometric luminosity distributions. The whole sample and the AO observed sub-sample are not statistically different with regards to spectral index or bolometric luminosity at the 3 σ level.

3.4. Target Fields

Figure 6 shows a 20'' \times 20'' (3000 AU to 10⁵ AU, depending on distance) field around each target at L'³. For targets where multiple near-IR sources do not fit within this field, more than one field is shown. Each near-IR source is labeled with a number that corresponds to that object's photometry presented in Table 4 if there is more than one object in the field.

³This figure could not be included in the astro-ph upload due to their file size limit. This paper with all figures can be downloaded from <http://homepage.mac.com/mconnelley/FileSharing1.html>. Thank you.

Inset images show regions of interest in more detail. In some cases, the primary star has been subtracted to better show a companion star in the inset image.

3.5. Photometry

We obtained H, K, and L'-band data in order to use the near-IR colors to separate embedded YSOs from foreground or background stars. We used archival CFHT Skyprobe data to ensure that the data we used for photometry were taken under photometric conditions, characterized by a stable attenuation measurement near 0 throughout the night. On nights that were non-photometric, the photometry was calibrated using field stars in our photometric data or in 2MASS. If we used 2MASS for H and K-band photometry and we have our own L' observations, the variability of our targets affects the accuracy of the colors that we derive, since the target may have varied in brightness between the 2MASS observations or between the 2MASS and our observations. We also converted the 2MASS photometry to the MKO system. Aperture photometry was performed using IMEXAMINE in IRAF using five aperture sizes (typically 0".9, 1".2, 1".5, 1".8, 2".1) while maintaining the same buffer and sky annulus width (both typically 1".8) for each aperture size. The same procedure was used for our standard stars. We compared the brightness of the target and the standard using the same aperture size to derive a magnitude estimate for each of the five aperture sizes. We then averaged these five estimates together, taking the standard deviation of these measurements as the accuracy to which we could measure the photometry of that individual source given the quality of the data. We made an airmass correction plot using our standard star data. We used the standard deviation of the standard star photometry from the best fit linear airmass extinction curve as the lower limit to our photometric errors. This error was combined with the individual measurement error via a Pythagorean sum (root of summed squares) to estimate the total photometric error for each object in each filter (δH , δK , and $\delta L'$ in Table 4). We used the airmass extinction values in Krisciunas et al. (1987) for our airmass correction.

4. Binary Detection

All binary stars were found by visual inspection of our images. We found that Fourier filtering of our PSF subtracted images (described below) did not enhance the visibility of close or faint companions since the PSF subtraction residuals had the same spatial size as a real companion. We did not attempt to use an automated star finding program on account of our previous experience with programs such as DAOFIND. As an example, if the search

parameters were set to find faint stars, then it would also identify positions without a star. Since our fields only had a few objects, a star finding program was not necessary.

4.1. Contrast Limit

Visual surveys for binary stars are always sensitive to contamination from background stars. One way to minimize background star contamination is by adopting a contrast limit, such that any star fainter than the limit is not considered as a potential companion since the possibility of such a faint star being background contamination is unacceptably high and the chance of it being a real companion is acceptably low. Haisch et al. (2004) used a contrast limit of $\Delta K=4$, whereas Reipurth & Zinnecker (1993) adopted a $\Delta z=5$ contrast limit. Duquennoy & Mayor (1991) found that nearly all main sequence binary stars with a solar-type primary have a mass ratio greater than 10:1. In light of this, we should choose an L' band contrast limit that allows for all binaries with a mass ratio greater than 10:1. Reipurth & Zinnecker (1993) state that for coeval stars on the Hayashi track, the flux ratio approaches the mass ratio as the wavelength increases, with these ratios being effectively equal at 2.2 μm . Consider a binary system with a mass ratio (and thus a photospheric flux ratio) of 10:1, where only the primary star has an infrared excess. In this case, the primary star's infrared excess can be up to three times greater than its photospheric flux without the observed flux ratio of the binary exceeding 40:1. Thus, a contrast limit of $\Delta L'=4$ satisfies our criteria for not excluding a significant number of real companions.

4.2. Artificial Binary Detection and the Inner Detection Limit

The angular resolution of the images, the contrast between the primary star and the companion, and to a lesser degree the plate scale of the camera affected how close we were able to detect a companion star. PSF fitting and subtraction was done with our L' data only to reveal very close and faint companions. The most successful PSF model was another field star in the same image. Since the image of the field star and target star were taken simultaneously, the PSFs of the two are nearly identical, and thus the field star is an excellent PSF model. However, this method could only be used rarely since the probability of another bright star being in the field of view is quite low. We usually used stars observed just before and just after the target to be subtracted, and combined these two PSFs into a model PSF for the one to be subtracted. The typical peak counts of the residual after PSF subtraction using this method are about 4% of the PSF's peak counts and are typically found about 1 FWHM from the center of the PSF. There were cases where a star had excessive PSF

residuals, either from a poor fit or due to scattered light off of circumstellar material at L' . Scattered light was much less of a problem at L' than at K but is still present, especially very close to the star. Excessive PSF residuals affected how close we could detect fake binary companions (described below), and this is reflected in our inner detection limits.

Knowing when companion stars could have been missed is nearly as important as detecting the companions themselves. Our data are less sensitive to close and faint companion stars. Thus, for each target, we needed to determine the closest separation that a companion of a given contrast could have been found so that we could later correct for our incomplete sensitivity to close and faint companions. To do this, we inserted artificial companions at a range of contrasts ($\Delta L' = 1, 2, 3,$ and 4 magnitudes fainter than the primary star) into the PSF subtracted image of each target star, regardless of whether it has a real binary companion. At each contrast level, we inserted 20 artificial companion stars, one at a time, at a known radius but at a random position angle into the PSF subtracted image. The image of each artificial binary was viewed for 1 s to ensure that we could easily and confidently find the artificial companion. The artificial companion also had to be easy enough to recover so that, if we were examining real data, we would confidently believe that we had found a companion star. Each artificial binary image was followed by an image of blank sky, also for 1 s, because we found that it was too easy to see the artificial companion “jump” around the image if images of artificial binary companions in different locations were viewed consecutively. If the companion could be recovered at least 19 out of 20 times, then the artificial companion would be inserted at a closer separation and the test repeated until the artificial companion could not be reliably recovered 95% of the time. The inner detection limit is determined to be the closest separation where the artificial companion could be reliably detected at least 95% of time. This test was repeated for each of the four contrast levels mentioned above, and for each individual star.

This method has the disadvantage that we know at what separation to expect artificial companions to be found. However, if we placed artificial companion stars at random separations and random position angles, most of the artificial stars would be inserted at a separation either too close to be recovered, or far enough away to be trivially detected. Even in the case where the artificial star is inserted at a random separation, we are most interested in artificial companions in the separation range where it is possible but difficult to detect the artificial companion. The method we used has the advantages that it quickly identifies the inner separation limit, and it uses the same method used for identifying real binary companions. Table 5 lists the binary systems that we identified. Table 6 lists the inner detection limit for each star at four contrast levels, as well as the outer companion acceptance limit (described below) at each of the four contrast levels.

4.3. Outer Detection Limit

The purpose of imposing an outer separation limit, beyond which no object would be considered as a companion, is to ensure that all candidate companions are likely to be gravitationally bound companions to the primary star and to help eliminate background star contamination. Duchêne et al. (2004) used an outer limit of $10''$ (1400 AU at the distance of their targets). They argue that this outer limit is much smaller than the typical size of a typical core in the regions they observed, thus these binaries are likely to have formed from the collapse of the same core or filament. Reipurth & Zinnecker (1993) used an outer limit of 1800 AU. They argue that the typical star-to-star separation in a low density star forming region is $\sim 20,000$ AU, and is $\sim 10,000$ AU in a high density region such as the Trapezium cluster. As such, 1800 AU is an order of magnitude smaller than the typical star-to-star separations for the regions that the targets observed by Reipurth & Zinnecker (1993) are in, and thus they argue that these companions are likely to be gravitationally bound.

There are a handful of well known common proper motion binary stars with very wide separations that are believed to be gravitationally bound. Perhaps the first star to be recognized as a real binary (versus an optical double) is β Capricorni (Mitchell 1767), which has a projected separation of 9400 AU. ϵ Lyrae 1 and 2 have a common proper motion and a projected separation of 13,000 AU (Burnham 1978). While it is rare for a companion to have a separation in excess of 2000 AU, it is possible for such widely separated stars to be gravitationally bound. Furthermore, the mean velocity dispersion of CO gas in the Taurus clouds is 1.4 kms^{-1} , and the observed radial velocity dispersion of Class I protostars is consistent with this value (Covey et al. 2006). At this velocity, it would take 1.7×10^4 years, or roughly the Class 0 life time, to drift 5000 AU. Thus, close but gravitationally unbound stars should be more than 5000 AU apart by the time they are visible in the near-IR as Class I YSOs. We accept companions with projected separation as great as 5000 AU in order to include widely separated companions with confidence that they are likely to be gravitationally bound.

The probability of background star contamination within a projected separation of 5000 AU could exceed 5%, which we consider unacceptably high. This is particularly true in regions near the Galactic center. We used star counts in our L' data to estimate the probability of contamination for each target. We counted all stars in our L' images with near-IR colors consistent with field stars. Since there are many fields with no apparent field stars, we grouped these fields into seven regions of Galactic longitude and latitude to improve the count statistics. Having also derived the L' apparent magnitude distribution for all stars in all fields, we used the star counts in a given region to estimate the density of field stars less than $L' = 4$ magnitudes fainter than each of the primary stars in that region. We used

this density and Equation 1 from Correia et al. (2006) to estimate the radius from the star where the probability of contamination exceeds 5%. This angular radius is:

$$\theta = \sqrt{-\ln(1 - P)/\pi\Sigma} \quad (1)$$

where θ is the angular radius with the probability of contamination P (in our case, $P=0.05$), and Σ is the surface density of field stars in that region of Galactic longitude and latitude that are less than $L'=4$ magnitudes fainter than the YSO in question. If the 5% contamination radius has a projected radius less than 5000 AU, then the contamination limited radius was used as the outer limit for accepting companions. Otherwise, 5000 AU was used. Although the maximum chance of contamination is 5%, the average chance of contamination within the adopted outer separation limit is 3.0%. Thus we expect there are ~ 6 (189×0.03) stars identified as binary companions that are background contamination stars. We note that there are a number of fields where the stellar density is so high that we can not confidently identify which object in the field, if any, is the near-IR counterpart to the IRAS source. These targets were thrown out and not considered as having been observed.

4.4. Color Selection Criteria

The goal of observing our targets in three bands was to use the location of each star observed (target, candidate companion, or background star) on an H-K vs. K-L' color-color diagram to minimize the chance of background star contamination. The H-K vs. K-L color-color diagram is divided into three main regions: a region of forbidden colors to the left of the reddening vector from the main sequence, a region of colors consistent with a reddened T Tauri star, and a region of colors consistent with a protostar having an IR excess greater than a T Tauri star (the region for reddened main sequence stars is very narrow). The colors of unreddened T Tauri stars (in the CIT photometric system, not in the MKO system) were adopted from Meyer et al. (1997). The direction of the reddening vector was derived from interstellar extinction values (assuming $R=5$, characteristic of dense clouds) taken from Mathis (2000). Using these values, the H-K reddening is 0.079 per magnitude of $A(V)$ extinction, and the K-L (not MKO L') reddening is 0.066 per magnitude of $A(V)$ extinction. Thus, the reddening vector has a slope of 1.20 on the H-K vs. K-L color-color diagram.

We excluded those stars whose colors are consistent with a reddened or unreddened main sequence star or with forbidden colors, with due caution. The colors of a close companion star are difficult to determine accurately due to the proximity of the brighter primary star.

Photometric errors and variability affect the measured colors. Reflection nebulosity can strongly affect the observed colors of a star, especially at H and K bands. Nebulosity makes the star appear bluer, and may not be spatially resolved. The colors of a protostar can range from the forbidden region (if the near-IR flux is dominated by scattered light) to the region characteristic of objects with a strong IR excess. As such, the color information had to be used with other selection criteria, such as the proximity to the IRAS position and the presence of a spatially resolved reflection nebula, to decide if a star is likely to be an embedded YSO or background contamination. Star counts were used along with colors since colors alone are not sufficient to mitigate the chance of background star contamination.

4.5. Discovery Space

Choosing which candidate companion stars would be retained for further consideration depended on several factors. Stars with H-K and K-L' colors near 0 are likely to be foreground stars and were excluded. An optical or IR reflection nebula is a clear sign that the object in question is physically associated with the cloud. Accurate colors often could not be determined for very close companions. Given the very low probability of contamination at such close separations, these candidate companions were kept.

Figure 7 shows the range of separations and contrasts over which we actually found binary companions. The number of companions versus $\log(\text{separation}/1'')$ is relatively constant. When plotted against linear separation (arcseconds), most of the binaries have separations less than $3''$. Also, for most of the range of separations, we are not less sensitive to fainter companions than brighter ones. It is only within a few times the FWHM (typically less than $1''$) that we are less sensitive to faint companions due to the glare of the primary star and, in a few cases, nebulosity. At wider separations, we can be less sensitive to faint companions since our data are not always deep enough to detect companions $\Delta L' = 4$ fainter than the primary star.

5. Binary Color Differences

A large number of our binary systems have very different colors between the two components, a situation analogous to the infrared companions of T Tauri stars. The prototypical case, T Tauri N and S, differ in their H-K colors by 1.39 magnitudes and in their K-L colors by 2.0 magnitudes (Ghez et al. 1991). Zinnecker & Wilking (1992) estimated that roughly 10% of T Tauri binary stars have an IR companion.

To find Class I analogues to T Tauri IR companions, we considered the difference in H-K and K-L' colors between the components of binary systems. This examination is limited to objects for which we have photometric data and where the binary is sufficiently well resolved that we have accurate photometry on each component. We were able to derive 49 H-K color differences and 59 K-L' color differences. The color difference distributions are shown in Figure 8. Both color difference distributions are centered near a color difference of 0, with the median $\Delta(\text{H-K})=0.016$, and the median $\Delta(\text{K-L}')=0.245$. The $\Delta(\text{K-L}')$ distribution is slightly wider than the distribution of $\Delta(\text{H-K})$, the standard deviations being 1.11 and 0.89, respectively. Thus, there is no statistically significant preference towards the primary star (defined as the brightest star at L') or the companion being redder. We find that 6/59 ($10.2\%_{-3.9\%}^{+5.6\%}$) of our Class I binaries have a K-L' color difference more extreme than the T Tauri system, and 9/56 ($16.1\%_{-5.0\%}^{+6.4\%}$) have a H-K color difference more extreme than the T Tauri system, including 7 targets where we have a lower limit on the H magnitude of one of the components. We note that only scattered light was detected at H and/or K-band for several targets, which naturally affects the observed colors. We find that protostellar analogues to T Tauri IR companions are quite rare. These values are consistent with the fraction of T Tauri stars that have an IR companion, suggesting a similar origin.

6. Summary

We have presented the results of a near-IR survey for binary stars in a new sample of nearby Class I protostars. The purpose of this paper is to make our observations available to the community, to stimulate follow-up research on these protostars, and to present data on protostellar binary stars for detailed statistical analysis that is presented in Paper II. This survey is distinguished by its well determined sample properties, large sample size, and choice of using L' observations to identify protostellar binary companions. We found 89 companion stars to 189 primary stars, 78 of which are within a projected separation of 5000 AU and have a contrast less than $\Delta L'=4$ magnitudes. We have empirically determined our companion detection limits to account for our incomplete sensitivity to binary companions. Separation and contrast limits were chosen to minimize the chance of background star contamination. The average chance of background star contamination is 3.0%, and we expect there are 6 stars identified as binary companions that are contamination. Near-IR colors were used to identify contaminant stars and we showed that infrared companions are as rare among Class I YSOs as they are among T Tauri stars.

Acknowledgments We thank the referee for helpful comments. This research has made use of the SIMBAD database, operated at CDS, Strasbourg, France. This research has made

use of NASA's Astrophysics Data System. This publication makes use of data products from the Two Micron All Sky Survey, which is a joint project of the University of Massachusetts and the Infrared Processing and Analysis Center/California Institute of Technology, funded by the National Aeronautics and Space Administration and the National Science Foundation. This research was supported by an appointment to the NASA Postdoctoral Program at the Ames Research Center, administered by the Oak Ridge Associated Universities through a contract with NASA.

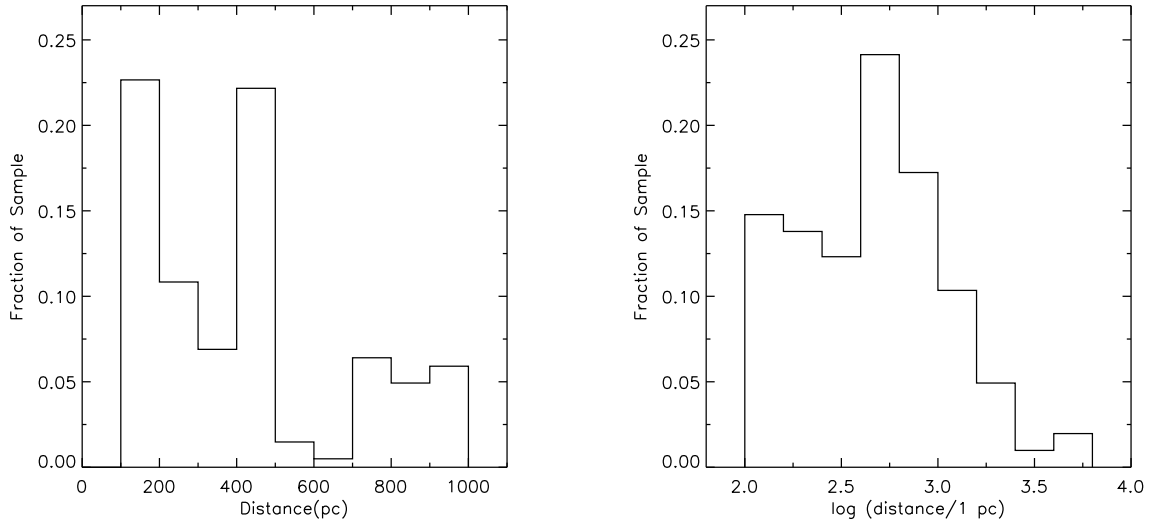


Fig. 1.— Distance distribution for our sample. The left panel shows the distance distribution for our sample on a linear scale out to a distance of 1 kpc. The right panel presents the same data on a log scale, including targets as far as 6 kpc. Our sample has a median distance of 470 pc and most objects are within 1 kpc.

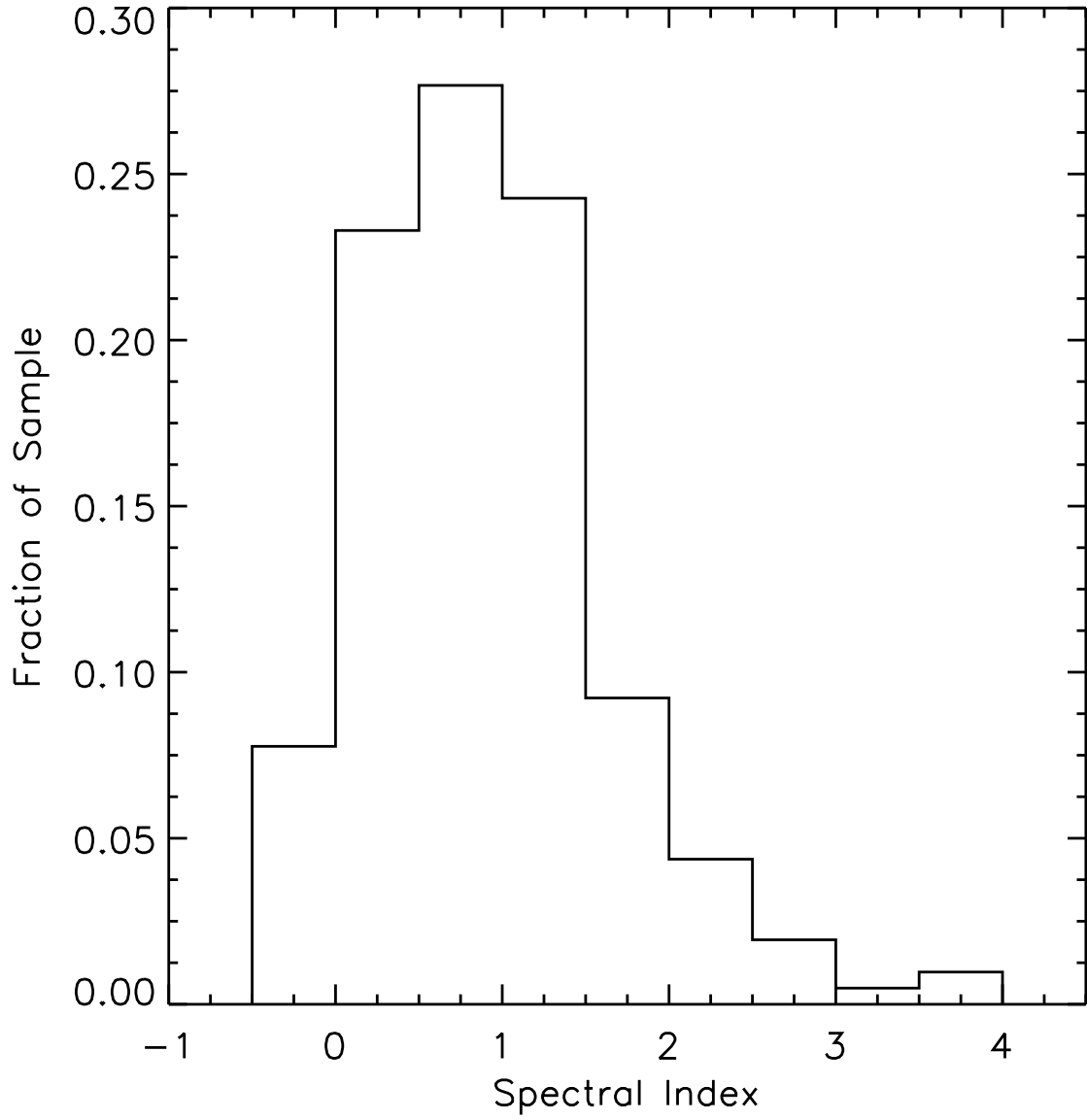


Fig. 2.— Spectral index distribution. IRAS $12\ \mu\text{m}$ to $100\ \mu\text{m}$ fluxes were used to calculate the spectral index, using the method described by Lada (1991). Our sample has a median spectral index distribution of $+0.79$, thus nearly all of our sources are Class I YSOs.

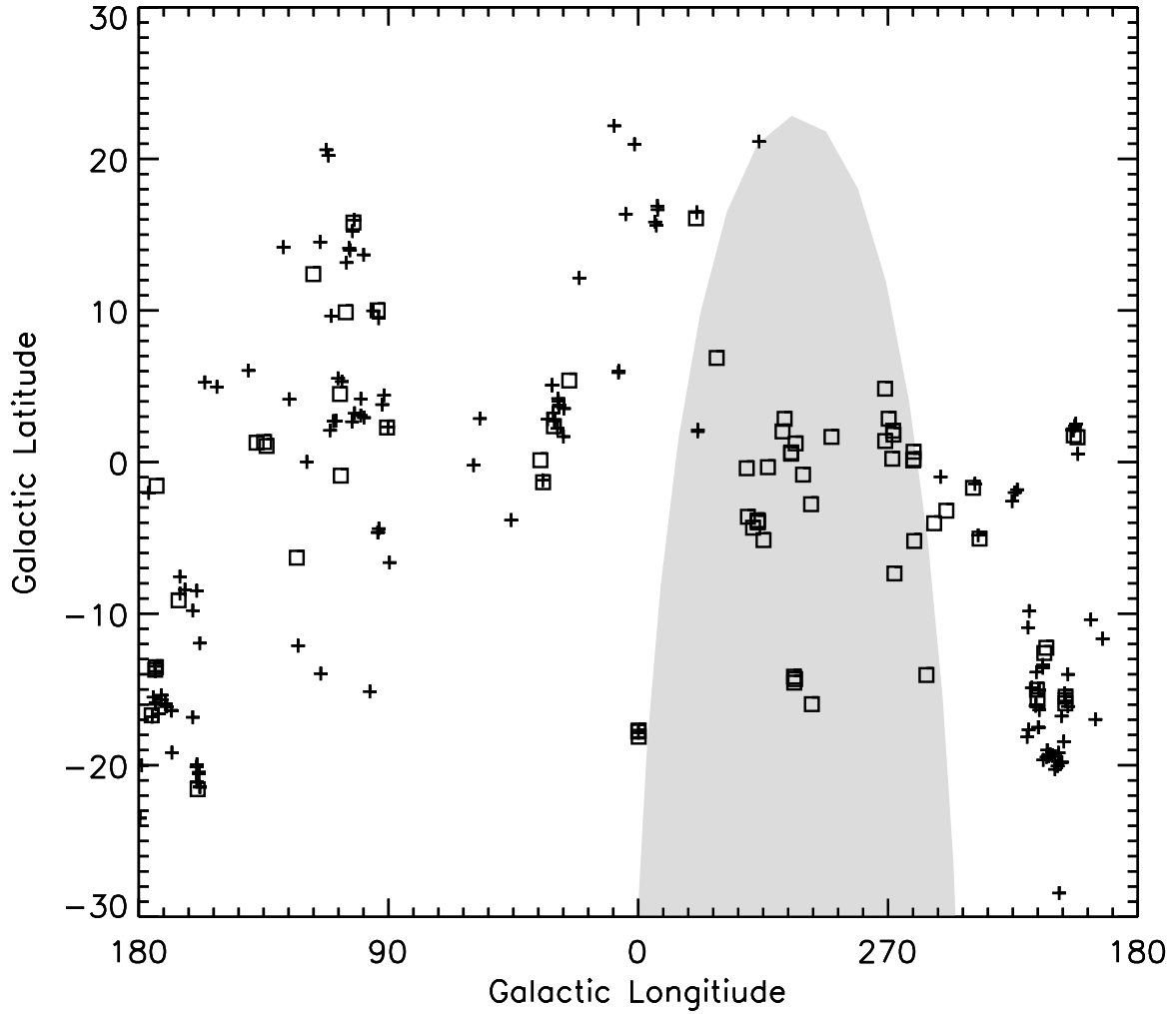


Fig. 3.— Location of our Class I sources in Galactic coordinates. The crosses are the targets we observed and the squares are targets that we did not observe, usually because they are too far south, there is no embedded near-IR counterpart to the IRAS source, or the source is an embedded cluster. The shaded area to the right is south of $\delta = -40^\circ$, and never rises above 2 airmasses from Mauna Kea. All of our targets are within 30° of the Galactic plane.

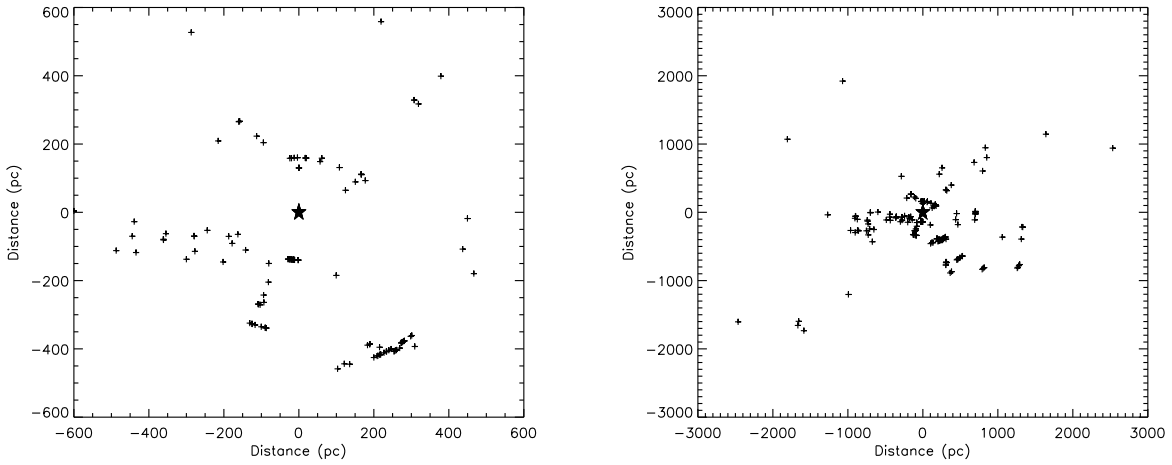


Fig. 4.— Location of our Class I sources looking down on the Galactic plane. The left panel shows sources out to a radius of 600 pc while the right panel shows sources out to a radius of 3 kpc. The Sun is represented by the star symbol in the center of the figure. The Galactic center is towards the top, the Taurus star forming region is just below the Sun, and the Orion star forming region is to the lower right.

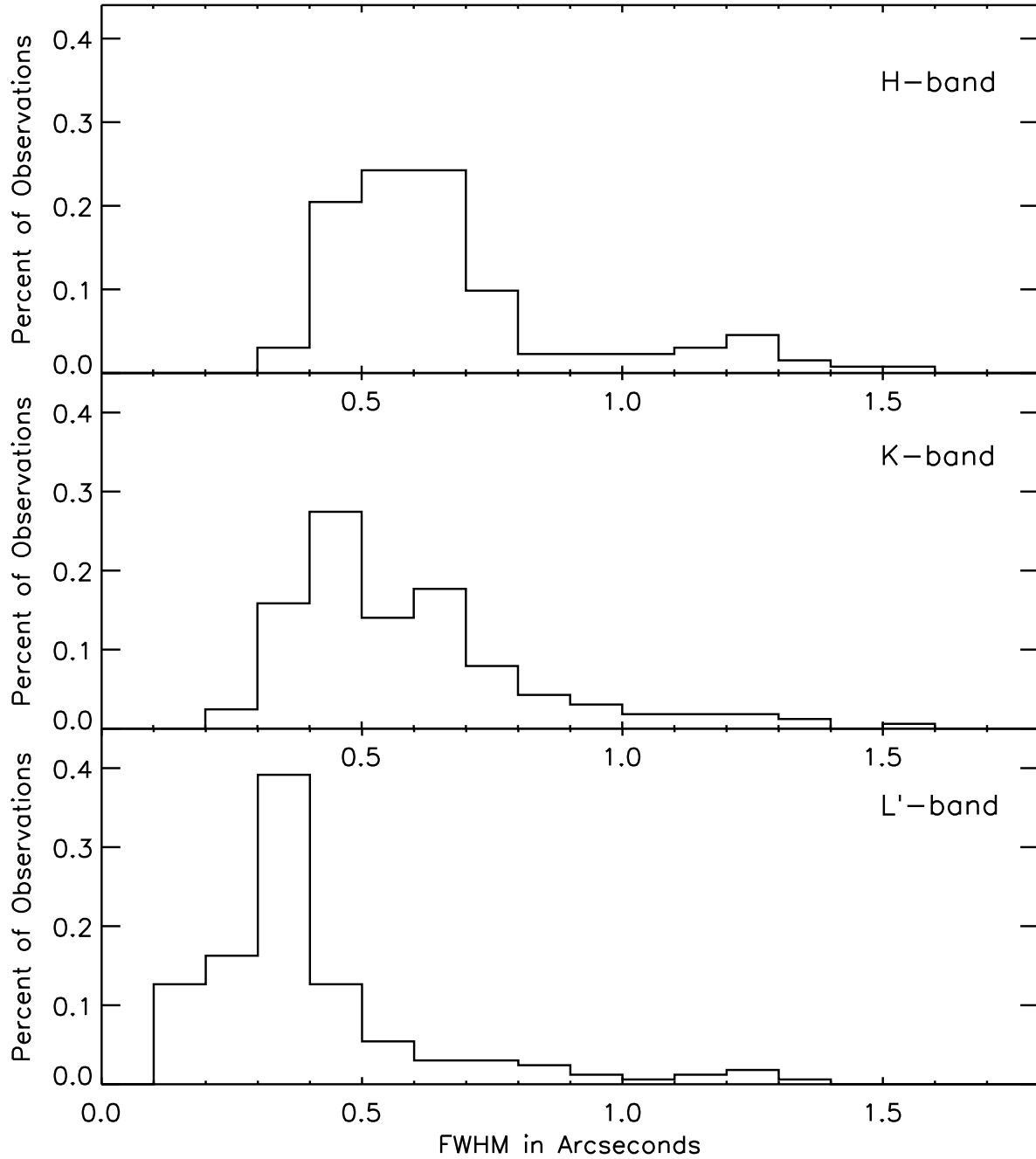


Fig. 5.— Angular resolution distributions at H, K, and L'. The median angular resolution (FWHM) is $0''.609$ at H, $0''.543$ at K, and $0''.335$ at L'.

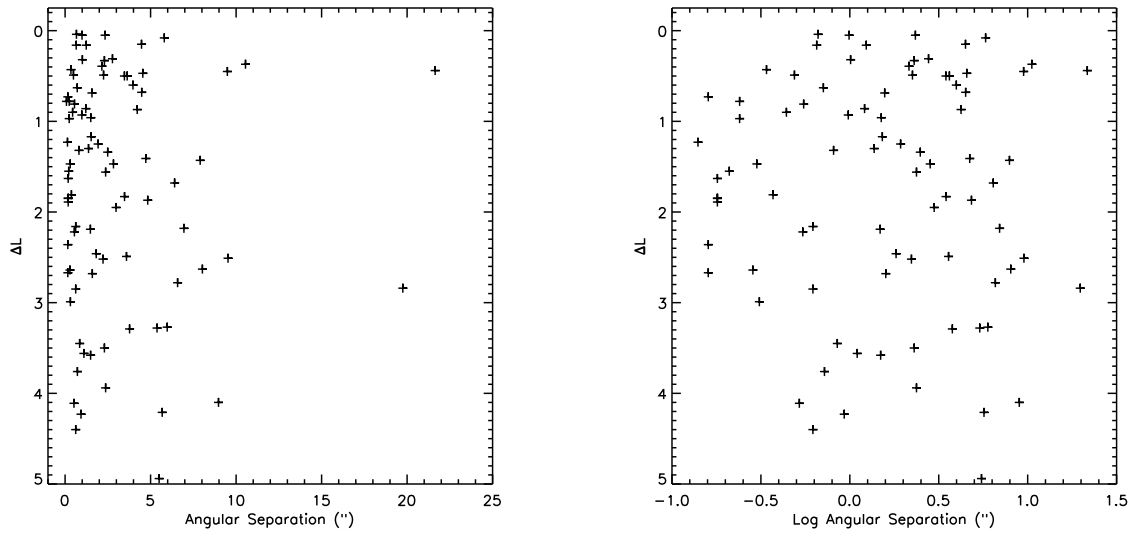


Fig. 6.— Discovery Space. These figures show the contrast of Class I binary companions versus angular separation (left) and versus $\log(\text{angular separation}/1'')$. We only appear to be losing binary companions at a contrast higher than $\Delta L' = 3$ and closer than $0''.5$.

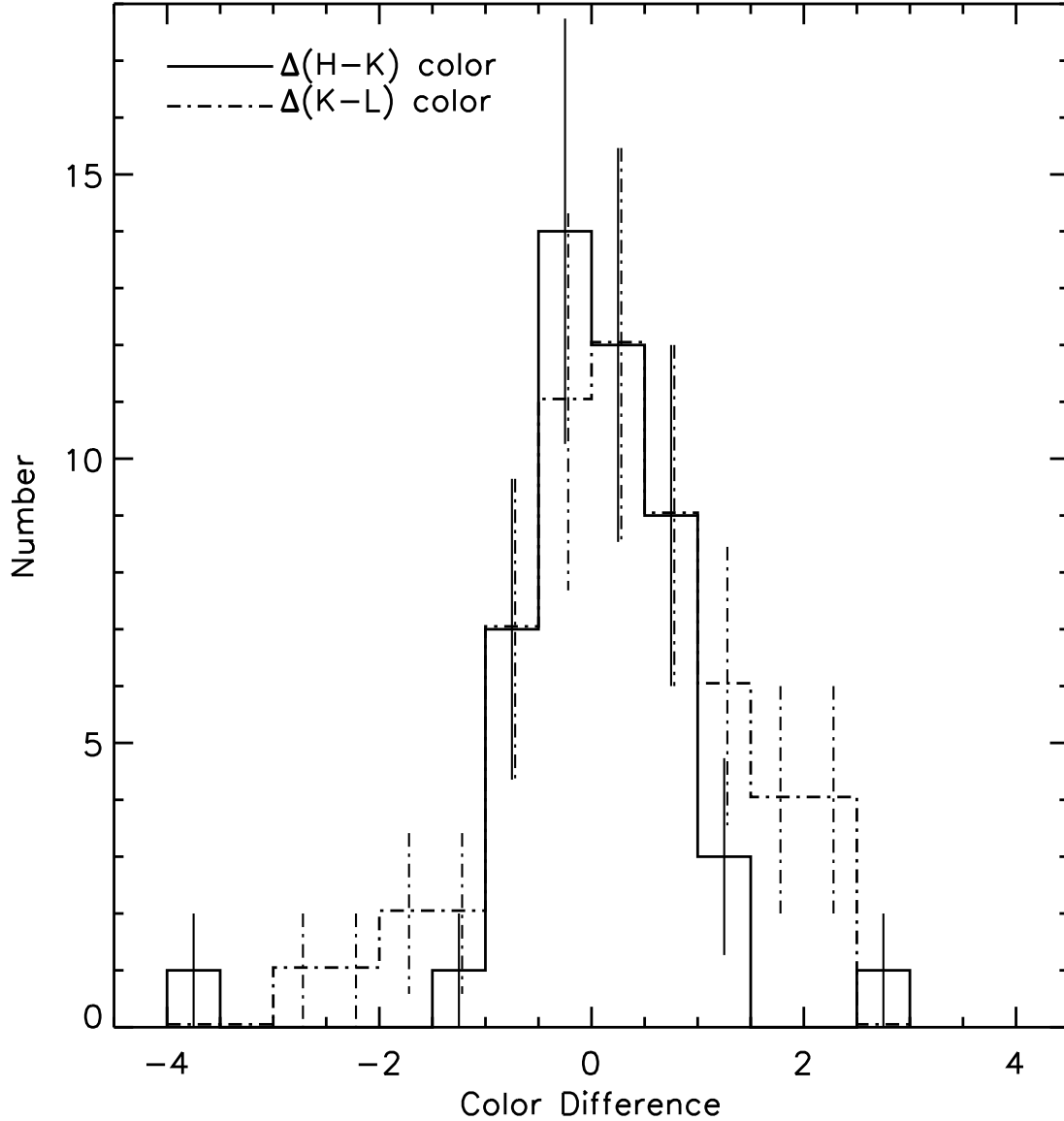


Fig. 7.— The H-K and K-L' color difference distributions. Both distributions are centered near a color difference of 0. 16% of H-K color differences and 10% of K-L' color differences have color differences greater than the T Tauri system. This percentage of Class I binaries with strong color differences is similar to the fraction of T Tauri stars with IR companions. This figure does not include objects where we only have a lower limit on the H-band magnitude.

Table 1. Source Characteristics

IRAS	Associations	D(pc) ^a	L_{bol}	α (J2000) ^b	δ (J2000) ^b	J ^c	H ^c	K_s ^c	α^d
00182+6223	L1280	4680(4)	366.9	00 20 56.79	+62 40 21.0	15.688	13.982	12.443	1.53
00465+5028	CB6, LBN 613	800(6)	8.8	00 49 24.50	+50 44 43.6	13.822	12.297	11.531	1.01
00494+5617	cluster in NGC 281	2940(21)	9854.4	00 52 23.7 ^I	+56 33 45	2.14
01166+6635		249(4)	0.4	01 20 03.93	+66 51 35.9	16.029	14.037	12.606	0.38
02086+7600	L1333	180(5)	0.8	02 13 43.61	+76 15 06.0	13.715	12.254	11.193	0.88
02232+6138	cluster	2040(46)	74578.	02 27 01.0 ^I	+61 52 14	1.76
02310+6133	IC 1805	2350(22)	1029.9	02 34 48.79	+61 46 44.5	13.864	1.64
02511+6023	S190 HII	2000(23)	485.6	02 55 01.99	+60 35 41.7	...	14.827	12.698	1.18
03220+3035	L1448 IRS 1, RNO 13	290(1)	2.0	03 25 09.43	+30 46 21.6	12.546	10.896	9.819	0.02
03225+3034	L1448 IRS 3 RNO 14	290(1)	13.1	03 25 36.47*	+30 45 21.4	13.745	12.363	11.095	1.52
03245+3002	L1455 IRS 1, RNO 15 FIR	260(1)	7.9	03 27 38.83*	+30 13 25.0	1.91
F03258+3105		220(47)	32.3	03 28 59.31	+31 15 48.5	16.490	12.528	10.437	0.59
03260+3111	L1450, SVS 3	290(1)	138.4	03 29 10.38	+31 21 59.2	9.368	7.987	7.173	0.58
03260+3111(W)		290(1)		03 29 07.74	+31 21 57.5	...	13.802	10.428	...
03271+3013	in NGC 1333	290(2)	1.6	03 30 15.16	+30 23 49.4	14.259	0.86
03301+3057	Barnard 1 IRS	290(2)	3.0	03 33 16.68	+31 07 54.9	14.208	1.52
03301+3111	Barnard 1	290(2)	4.0	03 33 12.84	+31 21 24.1	12.132	10.155	9.002	0.31
03331+6256		1560(4)	58.2	03 37 28.45	+63 06 31.2	14.590	0.45
03445+3242	HH 366 VLA 1 Barnard 5 IRS 1 L1471	280(1)	3.8	03 47 41.60	+32 51 43.8	...	14.047	11.214	0.16
03507+3801	HH 462	350(1)	2.5	03 54 06.19	+38 10 42.5	12.474	10.863	10.098	0.22
03580+4053	L1443	none		04 01 24.7 ^I	+41 01 48	1.40
04016+2610	L1489 IRS, HH 360	140(1)	3.0	04 04 43.05	+26 18 56.2	12.655	10.861	9.199	0.31
04067+3954	L1459	350(1)	15.1	04 10 08.40	+40 02 24.6	13.767	11.478	9.844	1.17
04073+3800	L1473, HH 463	350(1)	22.6	04 10 41.09	+38 07 54.0	15.339	13.552	10.500	0.07
04108+2803(E)	L1495N IRS	140(1)	0.7	04 13 54.72	+28 11 32.9	16.481	13.376	11.063	-0.15
04113+2758		140(1)	1.1	04 14 26.27	+28 06 03.3	12.475	9.878	7.777	-0.13
04169+2702	L1495, near HH 391	140(1)	0.9	04 19 58.45	+27 09 57.1	16.528	12.554	10.428	0.53
04181+2655(N)	HH392	140(1)		04 21 07.95	+27 02 20.4	13.855	12.062	10.543	1.96
04181+2655		140(2)		04 21 10.39	+27 01 37.3	...	13.783	11.085	...
04181+2655(S)		140(1)		04 21 11.47	+27 01 09.4	16.222	12.647	10.340	...
04189+2650(E)	FS Tau A	140(3)		04 22 02.18	+26 57 30.5	10.705	9.244	8.178	...
04189+2650(W)	FS Tau B, HH 157, Haro 6-5B	140(3)	0.6	04 22 00.70	+26 57 32.5	15.082	13.351	11.753	-0.04
04191+1523		140(7)	0.4	04 22 00.44	+15 30 21.2	16.592	12.354	11.259	0.97
04223+3700	L1478	350(1)	2.7	04 25 39.80	+37 07 08.2	...	13.170	10.271	0.47
04239+2436	HH 300 VLA 1 L1524	140(1)	1.1	04 26 56.30	+24 43 35.3	14.323	11.530	9.764	0.09
04240+2559	DG Tau	140(1)	3.5	04 27 04.70	+26 06 16.3	8.691	7.722	6.992	-0.26
04248+2612	L1521D, HH 31 IRS2, Barnard 217	140(1)	0.3	04 27 57.30	+26 19 18.4	11.619	10.270	9.741	0.52
04275+3452(N)		350(2)	1.2	04 30 47.79	+34 59 16.4	...	14.989	13.512	0.76

Table 1—Continued

IRAS	Associations	D(pc) ^a	L_{bol}	α (J2000) ^b	δ (J2000) ^b	J ^c	H ^c	K_s^c	α^d
04275+3452(S)		350(2)		04 30 47.57	+34 58 24.3	...	15.151	13.440	...
04275+3531		350(1)	1.5	04 30 48.52	+35 37 53.2	15.268	0.51
04287+1801	L1551 IRS 5B, HH 154	140(1)	20.2	04 31 34.08	+18 08 04.9	12.230	10.550	9.255	0.76
04288+2417	HK Tau	140(1)	0.2	04 31 50.57	+24 24 18.1	10.451	9.253	8.593	0.30
04292+2422(E)	Haro 6-13	140(1)	0.6	04 32 15.41	+24 28 59.7	11.237	9.319	8.101	0.01
04292+2422(W)	L1529	140(1)		04 32 13.27	+24 29 10.8	13.364	9.906	8.124	...
04295+2251	L1536 IRS	140(1)	0.3	04 32 32.05	+22 57 26.7	14.889	11.982	10.141	0.13
04302+2247	HH 394, near L1536	140(1)	0.3	04 33 16.50	+22 53 20.2	13.489	11.772	10.876	1.34
04315+3617	L1483	350(2)	1.7	04 34 53.22	+36 23 29.2	12.503	10.838	9.616	-0.05
04325+2402	L1535 IRS, Barnard 18I	140(1)	0.7	04 35 35.39	+24 08 19.4	16.122	11.504	9.826	1.71
04327+5432	L1400, HH 378	170(1)	1.9	04 36 45.50	+54 39 04.5	16.437	13.974	12.618	0.84
04365+2535	TMC-1A, L1534	140(1)	1.9	04 39 35.19	+25 41 44.7	16.389	12.062	10.020	0.68
04368+2557	L1527 FIR, HH 192 VLA 1	140(1)	1.3	04 39 53.6 ^I	+26 03 05.5	2.35
04369+2539	LBN 813, Barnard 14 L1527	140(1)	1.3	04 39 55.75	+25 45 02.0	10.668	8.052	6.275	-0.49
04381+2540	TMC-1, L1534	140(1)	0.6	04 41 12.68	+25 46 35.4	16.076	12.954	11.254	0.64
04530+5126	L1438, V347 Aur, RNO 33	none		04 56 57.02	+51 30 50.9	9.990	8.825	8.062	0.05
04591–0856	IC 2118	210(8)	0.9	05 01 29.64	–08 52 16.9	11.359	10.341	9.933	0.62
05155+0707	HH 114	460(17)	11.8	05 18 17.30	+07 10 59.9	...	12.567	10.214	1.55
05198+3325	cluster in NGC 1893	6000(24)	13481.	05 23 08.3 ^I	+33 28 38	0.50
05256+3049		16500(4)	6417.3	05 28 49.86	+30 51 29.3	...	14.412	11.914	0.16
05283–0412	HH 58	460(25)	5.4	05 30 51.30	–04 10 32.2	13.628	1.00
05286+1203	S264	400(26)	14.4	05 31 27.79	+12 05 30.9	...	14.596	12.763	1.05
05289–0430		470(2)	7.1	05 31 27.09	–04 27 59.4	13.082	11.086	9.425	0.38
05302–0537	Haro 4-145	470(2)	42.7	05 32 41.65	–05 35 46.1	...	15.116	11.389	0.38
05311–0631	L1641, HH 83 VLA 1	470(3)	7.3	05 33 32.52	–06 29 44.2	13.358	11.487	9.749	0.23
05320–0300	RNO 45, S277	400(26)	5.4	05 34 31.09	–02 58 02.3	13.726	11.758	10.546	2.12
05327–0457(N)		450(9)		05 35 14.39	–04 55 22.6
05327–0457(E)		450(9)		05 35 19.32	–04 55 45.0	15.547	12.277	10.079	...
05327–0457(S)		450(9)		05 35 14.99	–04 56 04.5	13.316	...
05327–0457(W)	Ced 55e	450(9)	920.2	05 35 13.10	–04 55 52.5	13.166	10.886	9.360	1.76
05340–0603		470(2)	19.3	05 36 32.48	–06 01 16.4	17.243	14.253	12.268	1.47
05357–0650	L1641	480(1)	10.8	05 38 09.31	–06 49 16.6	9.938	8.969	7.978	0.01
05375–0040	Haro 5-90	470(2)	7.1	05 40 06.79	–00 38 38.1	10.913	9.496	8.514	0.62
05375–0731	L1641 S3 IRS	480(1)	70.0	05 39 53.51	–07 30 09.5	...	14.662	12.497	2.13
05378–0750(W)	L1641	480(1)	8.2	05 40 14.95	–07 48 48.5	...	15.392	13.470	0.25
05378–0750(E)		480(1)		05 40 17.81	–07 48 25.8	15.939	12.647	10.488	...
05379–0758	L1641	480(1)	6.4	05 40 20.55	–07 56 39.9	12.851	10.678	9.399	0.19
05384–0808	L1641 S4, S85	480(1)	10.8	05 40 50.59	–08 05 48.7	13.134	11.349	10.276	1.03
05391–0841	L1641	480(1)	3.6	05 41 30.05	–08 40 09.2	...	14.729	11.855	0.77
05399–0121	L1630, HH 92,	430(1)	10.7	05 42 27.7 ^I	–01 20 02	1.53
05403–0818	L1641 S2	480(1)	9.9	05 42 47.07	–08 17 06.9	15.671	13.155	11.063	0.40

Table 1—Continued

IRAS	Associations	D(pc) ^a	L_{bol}	α (J2000) ^b	δ (J2000) ^b	J ^c	H ^c	K_s ^c	α^d
05404–0948	L1647	480(1)	49.8	05 42 47.67	–09 47 22.5	10.818	9.810	9.232	0.76
05405–0117	L1630	430(1)	4.4	05 43 03.06	–01 16 29.2	14.467	11.877	10.300	0.71
05413–0104	L1630, HH 212	430(1)	10.5	05 43 51.5 ^I	–01 02 52	2.91
05417+0907	L1594, HH 175, Barnard 35A	465(1)	18.4	05 44 30.01	+09 08 57.1	...	15.913	12.400	1.68
05427–0116		470(2)	2.5	05 45 17.31	–01 15 27.6	14.666	12.195	10.740	0.63
05450+0019	L1630	430(1)	27.6	05 47 36.55	+00 20 06.3	11.406	9.604	8.784	1.26
05510–1018		470(2)	1.8	05 53 23.71	–10 17 27.6	16.267	15.085	12.787	0.93
05513–1024		470(2)	5.1	05 53 42.55	–10 24 00.7	9.803	7.635	5.956	0.18
05548–0935		470(2)	1.1	05 57 13.23	–09 35 10.9	14.573	13.357	12.544	0.72
05555–1405(N)	RNO 58	470(2)	4.8	05 57 49.46	–14 05 27.8	13.711	12.190	11.014	0.62
05555–1405(S)		470(2)		05 57 49.18	–14 06 08.0	13.480	12.138	11.085	...
05564–1329		470(2)	5.6	05 58 46.91	–13 29 18.8	14.021	12.061	10.762	0.38
05580–1034		470(2)	1.7	06 00 24.49	–10 34 49.5	...	15.520	14.058	0.53
05581–1026		470(2)	2.9	06 00 28.64	–10 26 31.9	17.464	...	14.701	0.47
05582–0950	RNO 60	470(2)	3.9	06 00 38.76	–09 50 38.5	...	13.255	11.783	1.26
05596–0903		470(2)	2.3	06 02 01.7 ^I	–09 03 06	1.11
05598–0906(N)	GGD 10	470(2)	14.3	06 02 16.20	–09 06 29.0	14.553	11.876	9.813	0.43
05598–0906(S)		470(2)		06 02 15.52	–09 06 53.0	13.182	11.314	10.337	...
06010–0943	NGC 2149	425(20)	48.7	06 03 28.1 ^I	–09 43 57	1.50
06027–0714		830(1)	8.7	06 05 07.90	–07 14 42.6	16.226	13.473	12.607	1.08
06033–0710		830(1)	10.3	06 05 48.61	–07 10 31.2	1.28
06047–1117		500(10)	4.9	06 07 08.50	–11 17 51.0	14.119	12.222	10.220	0.64
06053–0622	Mon R2	830(19)	29143.	06 07 46.7 ^I	–06 23 00	0.74
06057–0923		830(2)	7.0	06 08 05.29	–09 23 47.3	0.97
06216–1044		830(2)	7.1	06 24 01.78	–10 45 53.5	...	14.365	11.614	0.14
06249–0953	L1652	830(1)	6.4	06 27 17.34	–09 55 27.4	15.034	13.652	12.559	1.04
06297+1021(E)		900(2)	46.8	06 32 30.83	+10 18 39.6	13.640	11.095	9.244	0.32
06297+1021(W)		900(2)		06 32 26.12	+10 19 18.4	10.884	9.316	8.025	...
06368+0938	L1613	790(11)	6.5	06 39 32.09	+09 35 41.5	0.93
06381+1039		960(4)	143.6	06 40 58.15	+10 36 52.1	14.513	1.93
06382+0939	NGC 2264 IRS 2 cluster	910(18)	512.6	06 41 02.7 ^I	+09 36 10	1.13
06382+1017	L1610/1613 HH 124	800(3)	84.4	06 41 02.64	+10 15 02.1	13.362	12.218	10.592	1.00
06393+0913		950(4)	28.9	06 42 08.13	+09 10 30.0	15.243	12.048	10.593	1.42
07018–1005(E)		1150(2)	30.3	07 04 13.93	–10 10 13.6	14.764	12.560	10.866	0.35
07018–1005(W)		1150(2)		07 04 09.86	–10 10 18.7	15.800	13.135	11.868	...
07025–1204(N)		1150(27)		07 04 50.71	–12 09 14.8	13.622	11.985	10.708	...
07025–1204(S)		1150(27)	49.5	07 04 51.62	–12 09 29.9	...	13.865	11.832	1.29
07028–1100		1150(2)	190.0	07 05 12.69	–11 04 29.9	16.847	14.155	12.242	0.96
07161–2336		1500(29)	30.2	07 18 15.65	–23 41 32.8	...	15.189	14.079	1.86
07178–4429		450(28)	18.1	07 19 28.26	–44 35 11.5	8.579	7.285	6.080	–0.28
07180–2356	L1660, HH 72 IRS	1500(17)	186.0	07 20 08.36	–24 02 23.0	...	14.176	11.648	0.81
07334–2320		1770(4)	30.2	07 35 34.51	–23 26 49.6	14.787	0.75
07339–2403	L1666	1790(4)	42.1	07 36 04.79	–24 10 17.1	14.066	0.68

Table 1—Continued

IRAS	Associations	D(pc) ^a	L_{bol}	α (J2000) ^b	δ (J2000) ^b	J ^c	H ^c	K_s ^c	α^d
07499–3306		1830(4)	42.9	07 51 50.8 ^I	–33 14 43	0.97
07576–3718		1370(4)	30.9	07 59 28.6 ^I	–37 26 33	1.44
08043–3343(N)		1120(4)	14.6	08 06 15.61	–33 52 19.5	...	15.274	13.016	0.39
08043–3343(S)		1120(4)		08 06 15.32	–33 52 35.3	...	15.937	13.985	...
08128–4357		none		08 14 33.97	–44 07 05.3	13.016	11.453	10.439	0.01
08261–5100		450(30)	4.8	08 27 39.00	–51 10 39.3	12.562	10.520	9.043	0.09
08373–4059		1340(4)	107.9	08 39 12.0 ^I	–41 10 05	0.99
08375–4109		700(12)	284.0	08 39 19.93	–41 19 50.5	...	12.980	9.470	0.68
08393–4041		1350(48)	361.4	08 41 06.76	–40 52 17.4	9.273	8.236	7.471	1.40
09049–4650		700(50)	13.6	09 06 39.0 ^I	–47 02 12	2.04
09099–4526	VdBH 29a	700(50)	13.7	09 11 46.86	–45 38 56.1	12.206	10.385	9.609	0.95
09116–4522		700(50)	9.0	09 13 27.44	–45 34 33.3	16.132	13.440	11.931	0.64
09204–4752		700(50)	169.0	09 22 12.49	–48 05 03.8	10.998	8.730	7.147	0.60
09212–4556		700(50)	6.7	09 23 02.1 ^I	–46 09 13	–0.08
09343–4522		700(50)	3.0	09 36 14.08	–45 36 04.5	0.64
11072–7727	Ced 111 IRS 5, HH 909 Chamaeleon IR Nebula	140(31)	14.3	11 08 38.20	–77 43 51.1	11.535	11.788	8.404	0.44
11101–5829	HH 136	2700(32)	11540.	11 12 18.19	–58 46 20.8	12.212	9.966	8.646	1.08
11590–6452		200(33)	9.0	12 01 36.40	–65 08 55.7	15.251	14.030	11.315	1.48
12277–6319		175(34)	6.6	12 30 34.5 ^I	–63 36 23	1.08
12512–6122		none		12 54 18.1 ^I	–61 38 19	0.83
12571–7654		200(35)	0.3	13 00 55.3 ^I	–77 10 40	0.23
13030–7707		200(35)	0.2	13 06 57.45	–77 23 41.5	10.841	9.579	8.755	–0.15
13036–7644		200(35)	1.0	13 07 36.1 ^I	–77 00 05	1.20
13050–6154		2000(36)	1174.0	13 08 12.25	–62 10 25.0	12.018	1.43
13054–6159		4000(51)	104106.	13 08 35.39	–62 15 06.9	15.393	13.183	11.875	1.32
13224–5928		1000(37)	45.6	13 25 41.36	–59 43 47.3	12.846	10.874	9.399	0.57
13294–6011		none		13 32 42.67	–60 26 54.2	...	12.861	10.763	1.21
13547–3944		550(38)	79.1	13 57 43.95	–39 58 47.1	8.865	8.069	7.264	0.62
14159–6111		1170(26)	4073.1	14 19 42.86	–61 25 12.1	...	14.080	11.583	1.78
14451–6502	VdBH 63	450(34)	6.0	14 49 17.6 ^I	–65 15 22	0.32
14563–6301		450(34)	10.2	15 00 22.71	–63 13 25.3	10.993	9.354	8.216	0.36
14564–6254	HH 77	450(34)	28.2	15 00 37.15	–63 06 52.2	16.455	13.184	10.887	1.03
14568–6304	HH 139	1000(3)	85.6	15 00 58.58	–63 16 55.0	11.733	10.064	8.763	–0.31
15107–5800		none		15 14 41.20	–58 11 49.9	15.909	12.319	8.507	1.83
15115–6231		1260(39)	66.5	15 15 41.08	–62 42 38.1	13.079	11.141	10.293	1.38
15215–6056		170(??)	0.5	15 25 39.6 ^I	–61 06 51	1.50
15398–3359	HH 185, Lupus 1, Barnard 228	170(3)	1.4	15 43 01.32	–34 09 15.3	15.963	13.992	12.326	1.59
15420–3408	HT Lup	159(49)	1.2	15 45 12.86	–34 17 30.6	7.573	6.866	6.480	0.00
15420–4553		none		15 45 37.02	–46 02 30.9	13.834	11.613	10.097	0.28
16235–2416	ρ Oph S1	160(1)	159.7	16 26 34.17	–24 23 28.3	8.859	7.261	6.317	1.34
16240–2430(E)	L1681	160(1)	25.6	16 27 09.43	–24 37 18.8	16.788	11.049	7.140	0.24
16240–2430(W)		160(1)		16 27 02.34	–24 37 27.2	14.164	10.478	8.064	...
16288–2450(E)	L1689 IRS 5, ρ Oph S	160(1)	5.5	16 32 02.22	–24 56 16.8	...	13.813	10.726	0.70

Table 1—Continued

IRAS	Associations	D(pc) ^a	L_{bol}	α (J2000) ^b	δ (J2000) ^b	J ^c	H ^c	K_s ^c	α^d
16288–2450(W)	ρ Oph S	160(1)		16 31 52.98	–24 56 24.6	11.783	9.391	7.557	...
16289–4449	HH 57 IRS, V346 Nor	150(34)	5.9	16 32 32.19	–44 55 30.7	10.178	8.599	7.176	–0.04
16293–2422	ρ Oph East	160(1)	23.7	16 32 22.8 ^I	–24 28 33	3.69
16295–4452		150(34)	1.9	16 33 07.73	–44 58 24.7	...	15.086	12.270	0.79
16316–1540	L43, RNO 91	160(1)	11.4	16 34 29.29	–15 47 01.9	10.994	9.635	8.464	0.84
16442–0930	L260	160(1)	0.7	16 46 58.27	–09 35 19.7	14.316	12.339	10.721	0.22
16544–1604		160(40)	1.1	16 57 20.12	–16 09 36.6	13.921	1.98
17364–1946	L219	none		17 39 23.25	–19 47 54.7	13.757	0.96
17369–1945	L219	none		17 39 55.95	–19 46 35.6	...	14.994	12.305	0.37
17441–0433	L425	none		17 46 50.89	–04 34 33.7	16.700	15.270	13.325	0.50
18148–0440	L483 FIR	225(1)	11.1	18 17 29.8 ^I	–04 39 38	16.188	12.640	10.790	1.36
18250–0351	NZ Ser	280(41)	219.7	18 27 39.53	–03 49 52.0	6.127	4.387	3.041	0.20
18264–0143		none		18 29 05.31	–01 41 56.9	13.968	1.39
18270–0153(E)		none		18 29 38.92	–01 51 06.3	...	15.321	12.874	...
18270–0153(W)		none		18 29 36.69	–01 50 59.1	13.700	11.797	10.711	0.49
18273+0034		none	1.4	18 29 53.06	+00 36 06.4	16.256	13.349	11.855	1.15
18274–0212		none		18 30 01.36	–02 10 25.6	...	15.145	11.489	0.12
18275+0040		700(42)	3.4	18 30 06.17	+00 42 33.6	9.833	8.605	7.516	–0.19
18278–0212		none		18 30 27.28	–02 11 00.2	14.550	1.62
18318–0434		none		18 34 31.73	–04 31 30.9	15.141	12.170	10.709	1.04
18331–0035	L588, HH 109, HH 108 IRAS	310(3)	3.8	18 35 42.00	–00 33 22.1	16.347	13.911	11.738	2.02
18339–0224		2200(43)	313.5	18 36 34.33	–02 21 49.0	...	14.505	13.304	1.32
18340–0116		none		18 36 38.54	–01 13 35.4	13.028	1.10
18341–0113	L564	none		18 36 46.33	–01 10 29.5	14.849	11.974	10.229	0.91
18358–0112		none		18 38 25.41	–01 10 10.2	...	13.770	12.089	1.24
18383+0059		none		18 40 51.87	+01 02 12.9	14.892	11.748	9.602	0.50
18527+0203		none		18 55 14.82	+02 07 47.8	14.253	11.078	9.556	1.67
18558+0041		none		18 58 23.01	+00 45 34.2	16.968	13.338	11.346	1.24
18561+0032		none		18 58 40.9 ^I	+00 36 49	1.46
18577–3701	S CrA	130(44)	1.5	19 01 08.61	–36 57 20.1	8.194	7.051	6.107	–0.18
18583–3657	TY CrA	130(44)	21.6	19 01 40.82	–36 52 33.7	7.486	6.970	6.673	0.62
18585–3701	R CrA	130(44)	44.3	19 01 53.68	–36 57 08.2	6.935	4.951	2.858	0.12
18595–3712	ISO-CrA 182	129(13)	1.2	19 02 58.70	–37 07 34.1	...	15.881	14.498	1.83
19247+2238		none		19 26 51.33	+22 45 13.4	11.095	9.881	9.175	0.50
19266+0932	Parsamian 21 HH 221	300(3)	3.4	19 29 00.86	+09 38 42.9	11.205	10.485	9.763	0.37
19411+2306		2100(14)	3026.1	19 43 17.94	+23 14 01.6	13.946	11.548	9.596	1.11
20353+6742	L1152, HH 376	370(1)	1.4	20 35 46.33	+67 53 02.0	15.263	14.230	13.254	1.41
20355+6343	L1100	450(6)	2.5	20 36 22.86	+63 53 40.4	13.885	11.797	10.339	0.59
20361+5733	L1041	none		20 37 20.8 ^I	+57 44 13	1.91
20377+5658	L1036	440(1)	4.8	20 38 57.48	+57 09 37.6	13.925	11.226	9.507	0.32
20386+6751	L1157 IRS, HH 375 VLA 1	370(1)	5.5	20 39 06.6 ^I	+68 02 13	2.23
20436+5849		910(4)	24.0	20 44 49.3 ^I	+59 00 18	1.31
20453+6746	PV Cep, HH 215,	500(3)	63.7	20 45 53.94	+67 57 38.7	12.453	9.497	7.291	–0.32

Table 1—Continued

IRAS	Associations	D(pc) ^a	L_{bol}	α (J2000) ^b	δ (J2000) ^b	J ^c	H ^c	K _s ^c	α^d
	L1158								
20568+5217	L1002, HH 381 IRS	1270(4)	45.6	20 58 21.09	+52 29 27.7	11.544	9.813	8.305	0.62
20582+7724	L1228, HH 199	175(1)	1.2	20 57 12.94	+77 35 43.7	13.024	10.608	9.171	0.31
21004+7811	HH 198, RNO 129	300(3)	13.5	20 59 14.03	+78 23 04.1	9.437	7.530	6.319	0.20
21007+4951	L988	700(1)	31.1	21 02 23.85	+50 03 06.8	16.368	14.818	13.276	0.69
21017+6742(E)	L1172	288(15)		21 02 29.94	+67 54 08.3	15.022	12.035	10.415	...
21017+6742(W)	L1172	288(15)	0.5	21 02 21.27	+67 54 20.1	14.890	0.66
21023+5002	cluster	1420(4)	873.0	21 03 57.6 ^I	+50 14 38	0.00
21025+5221	none			21 04 07.45	+52 33 53.5	12.896	1.12
21025+6801	L1172B	288(2)	2.6	21 03 14.24	+68 12 14.2	14.710	12.669	11.789	1.14
21169+6804	L1177, CB 230	450(6)	7.3	21 17 38.69	+68 17 33.4	11.562	9.898	9.188	1.75
21352+4307	Barnard 158	600(6)	11.7	21 37 11.39	+43 20 38.4	...	15.877	12.915	0.17
21388+5622	HH 588	750(16)	96.5	21 40 28.98	+56 35 55.7	12.801	11.620	10.789	0.59
21391+5802	L1121, IC 1396N	750(16)	254.2	21 40 42.80	+58 16 01.1	...	15.642	14.155	2.15
21418+6552	cluster	1380(4)	3432.8	21 43 02.3 ^I	+66 06 29	1.15
21432+4719	HH 379 IRS	900(45)	26.1	21 45 08.23	+47 33 05.6	14.643	13.169	11.914	1.07
21445+5712	IC 1396 East	360(4)	18.5	21 46 07.12	+57 26 31.8	13.950	11.965	10.139	0.54
21454+4718	L1031B, V1735 Cyg	900(1)	106.7	21 47 20.66	+47 32 03.6	9.889	8.087	7.040	0.70
21461+4722		900(2)	7.0	21 48 00.4 ^I	+47 36 38	1.07
21569+5842	L1143	250(4)	1.0	21 58 35.90	+58 57 22.8	15.457	12.936	10.695	0.08
22051+5848	L1165, HH 354 IRS	750(3)	73.0	22 06 50.37	+59 02 45.9	11.370	10.248	9.682	1.15
22176+6303	L1240, RAFGL 2884, S 140 IRS1-3	910(1)	21313.	22 19 20.39	+63 19 38.5	12.304	9.298	6.135	0.87
22266+6845	L1221, HH 363	200(1)	1.8	22 28 02.99	+69 01 16.7	16.575	13.544	11.465	0.53
22267+6244	L1203	900(1)	311.2	22 28 29.4 ^I	+62 59 44	15.826	11.799	9.244	1.45
22272+6358(E)	L1206	950(1)	815.5	22 28 57.60	+64 13 37.5	13.728	10.530	8.250	1.76
22272+6358(W)		950(1)		22 28 50.83	+64 13 44.8	...	14.944	12.483	...
F22324+4024	V375 Lac, LkH α 233	880(3)	111.6	22 34 41.01	+40 40 04.5	11.294	10.307	8.921	0.08
22376+7455	L1251B 3, HH 189	330(1)	10.7	22 38 47.02	+75 11 34.7	13.194	1.09
22451+6154	L1211	1290(4)	822.5	22 47 02.12	+62 10 05.4	14.941	12.401	10.855	1.20
22457+5751	cluster	4460(4)	25778.	22 47 46.5 ^I	+58 07 19	1.19
22517+6215		1030(4)	58.8	22 53 40.5 ^I	+62 31 59	1.45
23037+6213(E)	Cep C	1190(4)	330.2	23 05 49.76	+62 30 01.2	12.510	10.408	9.045	1.23
23037+6213(W)		1190(4)		23 05 45.77	+62 30 21.5	15.853	14.988	12.923	...
23238+7401	L1262 SMM 1	200(1)	0.9	23 25 46.6 ^I	+74 17 38	1.23
F23591+4748	none			00 01 43.25	+48 05 19.0	13.322	11.592	10.404	0.60

^aThe estimated distance to each source in parsecs. The citation for the distance estimate is designated by the number in the parenthesis, and are as follows: 1) Hilton & Lahulla, 1995, A&AS, 113, 325; 2) Educated guess based on proximity to nearby objects; 3) Reipurth, A General Catalog of HH Objects, 1999 (<http://casa.colorado.edu/hhcat/>); 4) Wouterloot & Brand, 1989, A&AS, 80, 149; 5) Obayashi et al. 1998, AJ, 115, 2740; 6) Launhardt & Henning 1997, A&A, 326, 329; 7) André et al. 1999, ApJ, 513, 57; 8) Kun et al. 2001, PASJ, 53, 1063; 9) Mookerjea et al. 2000, ApJ, 539, 775; 10) Yun et al. 2001, A&A, 372, 33L; 11) Sagar & Joshi, 1983, MNRAS, 205, 747; 12) Moreira et al. 2000, AJ, 119, 2960; 13) Marraco & Rydgren 1981, AJ, 86, 62; 14) Guetter, 1992, AJ, 103, 197; 15) Straizys et al. 1992, BaltA, 1, 149; 16) Battinelli & Capuzzo-Dolcetta 1991, MNRAS, 249, 76; 17) Reipurth & Aspin 1997, AJ, 114, 2700; 18) Neri et al. 1993, A&AS, 102, 201; 19) Racine 1968, AJ, 73, 233; 20) Wilson et al. 2005, A&A, 430, 523; 21) Guetter & Turner 1997, AJ, 113, 2116; 22) Heyer et al. 1996, ApJ, 464, 175; 23) Karr & Martin 2003, ApJ, 595, 900; 24) Marco et al., 2001, AJ, 121, 2075; 25) Reipurth et al. 1993, A&A, 273, 221; 26) Sugitani et al. 1991, ApJS, 77, 59; 27) Sugitani & Ogura 1995, Ap&SS, 224, 571; 28) Sugitani & Ogura 1994, ApJS, 92, 163; 29) Launhardt & Henning 1997, A&A, 326, 329; 30) Vilas-Boas et al. 2000, ApJ,

532, 1038; 31) Cambresy et al. 1998, A&A, 338, 977; 32) Tamura et al. 1997, MNRAS, 287, 894; 33) Bourke, 2001, ApJ, 554, 91; 34) Gregorio-Hetem et al. 1988, A&AS, 76, 347; 35) Hughes & Hartigan 1992, AJ, 104, 680; 36) Sugitani & Ogura 1994, ApJS, 92, 163; 37) Henning & Launhardt 1998, A&A, 338, 223; 38) Maheswar et al. 2004, MNRAS, 355, 1272; 39) Mikami & Ogura 1994, MNRAS, 270, 199; 40) Huard et al. 1999, ApJ, 526, 833; 41) Bachiller et al. 2001, A&A, 372, 899; 42) Zhang et al. 1988, A&A, 199, 170; 43) Birkmann et al. 2006, ApJ, 637, 380; 44) Knude & Hog 1998, A&A, 338, 897; 45) Davis et al. 2001, MNRAS, 326, 524; 46) Hachisuka et al. 2006, ApJ, 645, 337; 47) Aspin & Sandell 1997, MNRAS, 289, 1; 48) Wouterloot & Brand 1999, A&AS, 140, 177; 49) Prato et al. 2003, ApJ, 584, 853; 50) Liseau et al. 1992, A&A, 265, 577; 51) Clark & Porter 2004, A&A, 427, 839; none = Searched for and could not find a distance estimate

^b2MASS coordinate for candidate YSO. When a near-IR counterpart could not be identified in the 2MASS images, a superscript “I” designates a IRAS coordinate

^cMagnitudes from the 2MASS extended source catalog, in the 2MASS photometric system.

^d α is the spectral index of the source (Lada 1991)

Note. — RNO designates objects in “Red and Nebulous Objects in Dark Clouds: a Survey”. (Cohen, 1980, AJ, 85, 29)

Table 2. Observing Nights

Date (UT)	Observatory	Instr.	Weather
Nov. 2-5, 2003	UKIRT	UIST	4 nights photometric
Nov. 29-30, 2003	UKIRT	UIST	1.5 nights lost
Feb. 11-15, 2004	UKIRT	UFTI	4 photometric half-nights
May 15-17, 2004	UKIRT	UIST	3 half-nights lost
May 24-25, 2004	UKIRT	UIST	2 half-nights, 0.25 night lost
May 26-29, 2004	IRTF	SpeX	36 hours, photometric
Jun. 19-21, 2004	UKIRT	UIST	0.5 night lost
Jul. 29, 2004	UH 2.2 m	QUIRC	1 night, photometric
Aug. 2, 2004	Subaru	IRCS	0.5 nights lost, poor seeing
Aug. 3-5, 2004	UH 2.2 m	QUIRC	3 nights, 1.75 nights lost
Nov. 5, 2004	IRTF	SpeX	0.5 nights, clear
Nov. 18, 2004	IRTF	SpeX	0.5 nights, clear
Dec. 4-9, 2004	IRTF	SpeX	5 half-nights, 1.5 nights lost, poor seeing
Dec. 30-31, 2004	UKIRT	UIST	1.5 nights, 1 night lost
Nov. 16-18, 2005	Subaru	CIAO	3 nights, 1 non-photometric

Table 3. AO Observed Sample

IRAS	r (″) ^a	B ^b	R ^b	I ^b	Date
04240+2559	1.4	10.13	8.97	7.65	14Nov05
04530+5126	0.5	17.80	13.69	11.35	14Nov05
05289-0430E	0.4	17.51	14.96	14.54	15Nov05
05289-0430W	17.1	17.51	14.96	14.54	15Nov05
05302-0537	27.5	16.83	14.42	13.13	14Nov05
05327-0457W	35.7	17.71	15.89	14.18	15Nov05
05357-0650	0.3	12.98	10.52	10.38	15Nov05
05375-0040	5.5	16.37	14.04	12.63	14Nov05
05384-0807	37.1	9.94	8.03	7.82	15Nov05
05404-0948	0.6	18.41	15.16	12.96	15Nov05
05513-1024	3.0	12.91	11.79	9.47	15Nov05
05555-1405N	6.1		11.26	9.62	15Nov05
05555-1405S	17.0		10.52	9.69	15Nov05
06297+1021W	0.5	19.29	15.95	14.11	15Nov05
06382+1017	17.3	17.38	14.09	14.53	14Nov05
07025-1204N	15.5	17.86	15.10	13.06	15Nov05
07025-1204S	5.2	17.86	15.10	13.06	15Nov05
08043-3343	33.1	14.37	13.11	12.54	15Nov05
19247+2238	10.7	17.24	14.35	12.72	14Nov05
20453+6746	1.8	16.86	15.72	11.10	14Nov05
20568+5217	0.3	19.90	13.74	12.13	15Nov05
21388+5622	15.4	17.61	13.97		15Nov05
21454+4718	1.9	20.70	16.11	12.95	15Nov05
22376+7455	0.1	16.18	14.65	13.55	15Nov05

^aThe separation from the guide star to the target

^bThe USNO magnitudes of the guide star

Table 4. Target Photometry

IRAS	# ^a	H	δH^b	date	K	δK^b	date	L'	$\delta L'^b$	date
00182+6223	1	14.71	0.14	28jul04	13.16	0.08	28jul04	11.36	0.05	01aug04
00182+6223	2	18.11	0.04	28jul04	15.39	0.05	28jul04	13.37	0.14	01aug04
00182+6223	3	15.11	0.05	28jul04	14.15	0.05	28jul04	13.01	0.08	01aug04
00465+5028		14.94	0.18	03nov03	12.65	0.08	04nov03	9.96	0.05	02nov03
		9.79	0.04	19jun04
01166+6635		13.60	0.06	28jul04	12.30	0.06	28jul04	10.69	0.04	01aug04
02086+7600		11.90	0.04	28jul04	10.99	0.05	28jul04
02310+6133	
02511+6023	
03220+3035	1	12.16	0.04	04nov03	10.83	0.05	01nov03	8.43	0.05	03nov03
03220+3035	2	11.41	0.04	04nov03	10.57	0.05	01nov03	9.56	0.09	03nov03
03225+3034		12.60	0.11	03nov03
F03258+3105	1	13.71	0.03	10feb04	11.28	0.05	10feb04	9.32	0.05	29dec04
		13.67	0.04	29dec04	11.42	0.11	29dec04
F03258+3105	2	12.95	0.04	10feb04	10.88	0.05	10feb04	9.32	0.05	29dec04
		13.01	0.04	29dec04	11.00	0.12	29dec04
03260+3111	1	8.48	0.04	04nov03	7.67	0.05	01nov03	7.22	0.05	02nov03
03260+3111	2	9.06	0.04	04nov03	8.65	0.08	01nov03	7.85	0.08	02nov03
03260+3111	3	11.93	0.12	04nov03	10.88	0.08	01nov03	10.26	0.15	02nov03
03260+3111(W)		14.01	0.08	04nov03	10.12	0.10	01nov03	6.06	0.05	02nov03
03271+3013		17.07	0.15	04nov03	13.93	0.12	01nov03	11.29	0.07	02nov03
		16.84	0.12	10feb04	13.82	0.10	10feb04
03301+3111		12.35	0.04	13feb04	10.58	0.05	13feb04	7.72	0.04	29dec04
03301+3057		17.14	0.04	04nov03	13.53	0.18	01nov03	10.03	0.06	02nov03
03331+6256	1	17.72	0.16	28jul04	14.69	0.08	28jul04	11.73	0.07	01aug04
03331+6256	2	18.23	0.18	28jul04	15.00	0.05	28jul04	11.72	0.04	01aug04
03331+6256	3	16.58	0.06	28jul04	15.50	0.06	28jul04	14.82	0.04	01aug04
03445+3242		14.42	0.06	04nov03	11.49	0.06	01nov03	7.55	0.04	03nov03
03507+3801		11.21	0.04	04nov03	9.91	0.06	01nov03	8.08	0.04	03nov03
04016+2610		12.97	0.04	04nov03	10.39	0.29	01nov03	6.65	0.05	02nov03
		12.58	0.04	13feb04	10.31	...	02nov03
		10.47	0.05	13feb04
04067+3954		>19.33	0.04	04nov03	15.42	...	01nov03	10.22	0.18	01nov03
04073+3800		12.49	0.11	04nov03	9.05	0.12	01nov03	5.47	0.05	03nov03
04108+2803(E)		13.38	0.04	2MASS	11.06	0.02	2MASS	9.36	0.06	29dec04
04108+2803(W)		11.52	0.02	2MASS	10.37	0.02	2MASS	8.96	0.05	29dec04
04113+2758	1	9.93	0.04	04nov03	8.20	0.05	02nov03	6.41	0.04	03nov03
04113+2758	2	9.48	0.04	04nov03	8.27	0.05	02nov03	7.01	0.04	03nov03
04169+2702		14.24	0.04	2MASS	11.26	0.06	01nov03	8.31	0.04	03nov03
04181+2654(N)		7.97	0.05	29dec04
04181+2654		8.84	0.04	29dec04
04181+2654(S)		7.91	0.05	29dec04
04189+2650(E)		9.50	0.04	04nov03	8.28	0.06	02nov03	6.72	0.05	01nov03
04189+2650(W)		13.52	0.06	04nov03	12.03	0.07	02nov03	9.55	0.05	01nov03
04191+1523	1	14.33	0.11	04nov03	12.04	0.07	04nov03	9.25	0.05	02nov03
04191+1523	2	16.72	0.18	04nov03	14.35	0.08	04nov03	12.20	0.07	02nov03

Table 4—Continued

IRAS	# ^a	H	δH^b	date	K	δK^b	date	L'	$\delta L'^b$	date
04223+3700	1	13.29	0.04	04nov03	10.13	...	02nov03	7.14	0.05	01nov03
		13.37	0.06	11feb04	9.93	0.05	11feb04	6.86	0.04	29dec04
		13.50	0.04	13feb04	10.15	0.05	13feb04
04223+3700	2	14.47	0.05	04nov03	11.69	...	02nov03	10.79	0.08	01nov03
		14.82	0.10	11feb04	12.33	0.08	11feb04	10.60	0.07	29dec04
		14.60	0.05	13feb04	12.17	0.07	13feb04
04223+3700	3	>17.64	...	04nov03	14.50	0.09	02nov03	12.33	0.09	01nov03
		17.87	0.09	11feb04	14.74	0.06	11feb04	12.71	0.04	29dec04
		17.87	0.05	13feb04	14.79	0.07	13feb04
04239+2436	1	13.00*	0.07	04nov03	10.22*	0.05	02nov03	7.55	0.05	29dec04
04239+2436	2	13.00*	0.07	04nov03	10.22*	0.05	02nov03	9.26	0.05	29dec04
04240+2559		7.66	0.04	04nov03	6.78	0.05	02nov03	5.51	0.04	03nov03
04248+2612		11.50	0.04	04nov03	10.62	0.05	04nov03
04275+3452(N)	
04275+3452(S)	
04275+3531		19.58	0.04	04nov03	15.38	0.22	04nov03	11.77	0.10	03nov03
		18.61	0.21	10feb04
04286+1801(E)		8.62	0.11	29dec04
04286+1801(W)	
04288+2417	1
04288+2417	2	12.04	0.05	11feb04	11.58	0.05	11feb04
04292+2422(E)		7.63	0.05	02nov03	6.26	0.05	03nov03
04292+2422(W)		8.05	0.05	02nov03	7.01	0.04	03nov03
04295+2251		10.54	0.07	02nov03	8.70	0.05	03nov03
04315+3617	1	9.20	0.05	02nov03	7.56	0.04	03nov03
04315+3617	2	10.88	0.05	02nov03	10.06	0.08	03nov03
04325+2402	1	13.61	0.10	04nov03	11.29	0.05	04nov03	9.61	0.16	02nov03
		14.15	0.10	10feb04	11.92	0.05	10feb0
04325+2402	2	16.41	0.32	04nov03	14.03	0.05	04nov03	13.20	0.04	02nov03
		16.46	0.04	10feb04	14.33	0.05	10feb04
04327+5432		16.41	0.22	04nov03	14.00	...	02nov03	10.07	0.06	03nov03
04365+2535		13.43	0.13	04nov03	10.60	0.13	02nov03	7.10	0.05	03nov03
04369+2539	
04381+2540		14.16	0.03	11feb04	11.81	0.11	02nov03	8.94	0.11	03nov03
		11.74	0.07	11feb04
04530+5126		7.80	0.06	02nov03	6.67	0.05	03nov03
04591-0856		11.86	0.10	04nov03	10.40	0.07	02nov03	8.81	0.05	03nov03
05155+0707	1	13.34	0.07	11feb04	11.39	0.05	04nov03	9.58	0.06	01nov03
		11.41	0.05	11feb04
05155+0707	2	13.84	0.05	04nov03	11.80	0.19	01nov03
		13.78	0.05	11feb04
05256+3049	1	12.84	0.04	12feb04	10.17	0.05	02nov03
		10.44	0.06	12feb04
05283-0412	1	13.52	0.12	28jul04	10.76	0.07	29dec04
05283-0412	2	13.82	0.15	28jul04	11.10	0.06	29dec04
05286+1203	1	14.66	0.09	12feb04	12.98	0.06	02nov03	10.93	0.09	29dec04

Table 4—Continued

IRAS	# ^a	H	δH^b	date	K	δK^b	date	L'	$\delta L'^b$	date
		12.82	0.07	12feb04
05286+1203	2	13.43	0.04	12feb04	13.08	0.05	02nov03	12.61	0.05	29dec04
		12.95	0.07	12feb04
05286+1203	3	13.04	0.04	12feb04	12.87	0.05	02nov03	12.79	0.08	29dec04
		12.78	0.06	12feb04
05289-0430(E)	1a	11.13	0.03	2MASS	9.61*	0.05	02nov03	7.21	0.05	03nov03
		7.19	0.06	16nov05
05289-0430	1b	02nov03	9.34	0.05	03nov03
		9.74	0.05	16nov05
05289-0430(W)	2	10.52	0.02	2MASS	9.66	0.05	02nov03	9.23	0.05	03nov03
05302-0537	1	14.27	0.04	04nov03	10.39	0.06	04nov03	6.79	0.05	01nov03
		14.25	0.04	10feb04	10.22	0.05	10feb04	6.74	0.06	15nov05
05302-0537	2	15.42	0.10	04nov03	11.29	0.08	04nov03	6.95	0.05	01nov03
		15.83	0.04	10feb04	11.56	0.08	10feb04	7.32	0.05	15nov05
05311-0631	1	12.90	0.11	12feb04	10.14	0.07	04nov03	7.68	0.05	01nov03
		10.12	0.07	12feb04
05311-0631	2	11.28	0.05	12feb04	10.38	0.05	04nov03	10.09	0.13	01nov03
		10.39	0.06	12feb04
05320-0300	1	10.33	0.05	04nov03	8.61	0.07	04nov03
05327-0457(E)	
05327-0457(W)	1a	10.78*	0.04	04nov03	9.30*	0.05	...	8.17*	0.05	01nov03
		8.46	0.06	16nov05
05327-0457	1b	9.29	0.06	16nov05
05327-0457	2	15.20	0.09	04nov03	12.95	0.12	04nov03	11.67	0.07	01nov03
		15.19	0.05	10feb04	13.05	0.07	10feb04	11.96	0.16	16nov05
05327-0457	3	15.58	0.06	04nov03	13.64	0.15	04nov03	12.19	0.06	01nov03
		15.56	0.07	10feb04	13.52	0.08	10feb04	12.61	0.10	16nov05
05327-0457(N)	4	12.26	0.04	10feb04	11.86	0.06	10feb04	11.28	0.10	01nov03
		11.31	0.06	16nov05
05327-0457	5	13.45	0.05	04nov03	11.98	0.06	04nov03	11.15	0.07	01nov03
		13.49	0.05	10feb04	12.02	0.06	10feb04	11.03	0.06	16nov05
05327-0457(S)	6	15.38	0.13	04nov03	13.16	0.11	04nov03	11.58	0.05	01nov03
		15.38	0.04	10feb04	13.22	0.05	10feb04
05327-0457	7	16.46	0.03	04nov03	14.52	0.05	04nov03	12.13	0.07	01nov03
		16.86	0.04	10feb04	14.27	0.05	10feb04
05340-0603(E)	1	14.25	0.04	2MASS	12.27	0.03	2MASS
05340-0603(W)	2	>16.6	...	2MASS	14.94	0.09	2MASS
05357-0650	1	8.50	0.04	04nov03	7.93	0.03	2MASS	6.08	0.05	01nov03
		6.15	0.05	03nov03
		5.90	0.06	16nov05
05357-0650	2	13.23	0.16	04nov03	12.45	0.10	2MASS	11.90	0.16	01nov03
		12.25	0.08	03nov03
		11.95	0.05	16nov05
05357-0650	3	12.53	0.06	04nov03	11.93	0.03	2MASS	11.85	0.12	01nov03
		11.90	0.19	03nov03
		11.46	0.07	16nov05

Table 4—Continued

IRAS	# ^a	H	δH^b	date	K	δK^b	date	L'	$\delta L'^b$	date
05375-0731	3	15.63	0.06	12feb04	13.16	0.06	12feb04
05375-0731	4	14.99	0.04	12feb04	12.84	0.05	12feb04
05375-0040	1	9.52	0.04	2MASS	8.47	0.02	2MASS	7.32	0.06	15nov05
05375-0040	2	11.27	0.05	2MASS	10.24	0.03	2MASS	8.93	0.06	15nov05
05375-0040	3	10.57	0.04	2MASS	9.41	0.02	2MASS	8.25	0.05	15nov05
05378-0750(E)		12.58	0.05	12feb04	9.57	0.05	04nov03	7.52	0.06	01nov03
05378-0750(W)		15.82	0.14	12feb04	13.43	0.08	04nov03	10.85	0.05	01nov03
		13.34	0.08	12feb04
05379-0758	1	10.71	0.03	2MASS	9.35	0.03	2MASS	6.89	0.05	01nov03
05379-0758	2	11.99	0.03	2MASS	10.86	0.03	2MASS	9.46	0.05	01nov03
05379-0758	3	14.53	0.10	2MASS	12.29	0.04	2MASS	10.10	0.05	01nov03
F05384-0807	1	11.58	0.06	04nov03	9.33	0.05	01nov03
		11.48	0.06	11feb04	9.29	0.06	16nov05
F05384-0807	2	13.68	0.21	04nov03	11.12	...	01nov03
		13.07	0.05	11feb04	10.94	0.06	16nov05
F05384-0807	3	10.52	0.07	04nov03	8.61	0.05	01nov03
		10.38	0.07	11feb04	8.84	0.09	16nov05
F05384-0807	4	14.51	0.07	04nov03	11.33	0.05	01nov03
		14.25	0.06	11feb04	11.44	0.10	16nov05
F05384-0807	5	14.58	0.06	04nov03	11.63	...	01nov03
		14.37	0.06	11feb04	11.52	0.10	16nov05
F05391-0841	1	15.92	0.08	04nov03	12.13	0.05	02nov03	9.30	0.05	03nov03
		15.90	0.04	11feb04	12.21	0.05	11feb04
F05391-0841	2	14.60	0.06	04nov03	11.63	0.05	02nov03	8.92	0.05	03nov03
		14.86	0.04	11feb04	11.80	0.05	11feb04
F05391-0841	3	>17.53	0.03	04nov03	14.55	0.05	02nov03	12.17	0.09	03nov03
		18.02	0.06	11feb04	14.47	0.05	11feb04
05403-0818	1	13.22	0.04	2MASS	11.29	0.05	04nov03	8.36	0.04	02nov03
		7.97	0.06	04nov03
05404-0948	1a	9.76*	0.04	04nov03	9.23*	0.05	02nov03	8.93*	0.05	03nov03
		8.87	0.07	16nov05
05404-0948	1b	11.28	0.18	16nov05
05404-0948	2	13.84	0.08	04nov03	12.65	0.06	02nov03	11.61	0.05	03nov03
		11.49	0.06	16nov05
05405-0117	1	12.10	0.05	13feb04	10.25	0.05	02nov03	8.37	0.05	29dec04
		10.17	0.06	13feb04
05417+0907	1	16.11	0.07	04nov03	12.52	0.05	02nov03	9.35	0.07	03nov03
		16.14	0.06	10feb04	12.48	0.05	10feb04
05417+0907	2	18.06	0.24	04nov03	13.96	0.08	02nov03	10.48	0.05	03nov03
		18.13	0.04	10feb04	13.88	0.08	10feb04
05427-0116	1	12.48	0.06	04nov03	10.92	0.05	04nov03	8.66	0.08	04nov03
		12.34	0.04	11feb04	10.87	0.05	10feb04
05427-0116	2	14.03	0.10	04nov03	12.11	0.06	04nov03	10.12	0.11	04nov03
		13.99	0.07	11feb04	12.20	0.05	10feb04
05510-1018	1	15.85	0.07	04nov03	13.14	0.05	04nov03	10.99	0.05	03nov03
		15.57	0.12	10feb04	12.88	0.06	10feb04

Table 4—Continued

IRAS	# ^a	H	δH^b	date	K	δK^b	date	L'	$\delta L'^b$	date
05510-1018	2	15.89	0.03	04nov03	13.96	0.25	04nov03	11.09	0.11	03nov03
		15.48	0.04	10feb04	13.34	0.05	10feb04
05513-1024	1	7.68	0.04	2MASS	5.89	0.02	2MASS	3.56	0.05	16nov05
05513-1024	2	11.90	0.05	16nov05
05513-1024	3	11.18	0.05	16nov05
F05548-0935	1	14.44	0.10	04nov03	13.39	0.06	04nov03	13.15	0.11	03nov03
		14.21	0.04	13feb04	13.27	0.09	13feb04
F05548-0935	2	15.33	0.23	04nov03	14.10	0.16	04nov03	11.79	0.05	03nov03
		15.04	0.04	13feb04	13.62	0.05	13feb04
F05548-0935	3	14.18	0.05	04nov03	13.21	0.05	04nov03	12.40	0.06	03nov03
		14.32	0.06	13feb04	13.34	0.06	13feb04
05555-1405(N)	1a	12.22	0.04	2MASS	10.62	0.05	04nov03	9.22	0.05	03nov03
		9.21	0.05	16nov05
05555-1405	1b	12.09	0.07	03nov03
		10.64	0.05	16nov05
05555-1405	2	10.96	0.03	2MASS	9.93	0.05	04nov03	9.17	0.05	03nov03
		9.03	0.05	16nov05
05555-1405	3	10.22	0.02	2MASS	9.93	0.05	04nov03	10.03	0.05	03nov03
		9.78	0.05	16nov05
05555-1405(S)	4	12.16	0.02	2MASS	10.86	0.05	04nov03	9.26	0.05	03nov03
		9.23	0.05	16nov05
05564-1329	1	14.52	0.14	04nov03	11.82	0.07	04nov03	9.01	0.05	01nov03
		14.57	0.15	10feb04	11.89	0.07	10feb04
05564-1329	2	12.60	0.09	04nov03	11.17	0.06	04nov03	9.81	0.05	01nov03
		12.60	0.10	10feb04	11.18	0.07	10feb04
05580-1034		15.61	0.07	13feb04	13.87	0.05	04nov03	10.84	0.05	03nov03
05581-1026		16.69	0.03	13feb04	14.76	0.13	04nov03	12.10	0.13	02nov03
05596-0903		14.52	0.15	04nov03	10.94	0.12	29dec04
05598-0906(N)	1	12.16	0.08	11feb04	10.06	0.09	02nov03	7.50	0.05	03nov03
		10.06	0.07	11feb04
05598-0906	2	>15.34	0.03	11feb04	>13.14	0.05	11feb04	11.22	0.18	03nov03
05598-0906	3	13.96	0.04	11feb04	12.97	0.09	02nov03	12.12	0.07	03nov03
		12.82	0.05	04nov03
		12.96	0.06	11feb04
05598-0906(S)	4	11.30	0.03	11feb04	10.34	0.08	02nov03	9.79	0.05	03nov03
		10.27	0.05	04nov03
		10.30	0.05	11feb04
05598-0906	5	12.30	0.04	11feb04	11.70	0.05	04nov03	10.83	0.07	03nov03
		11.89	0.06	11feb04
05598-0906	6	13.46	0.05	11feb04	12.97	0.06	04nov03	12.14	0.10	03nov03
		13.01	0.08	11feb04
05598-0906	7	11.44	0.03	11feb04	10.84	0.05	04nov03	10.05	0.05	03nov03
		10.63	0.05	11feb04
05598-0906	8	14.77	0.03	11feb04	13.83	0.05	04nov03	13.84	0.05	03nov03
		14.15	0.09	11feb04
06027-0714		11.199	0.10	02nov03

Table 4—Continued

IRAS	# ^a	H	δH^b	date	K	δK^b	date	L'	$\delta L'^b$	date
06033-0710		17.08	0.14	12feb04	15.00	0.13	12feb04	13.107	0.20	03nov03
06047-1117		13.16	0.05	2MASS	10.32	0.02	2MASS	7.799	0.05	03nov03
06216-1044		14.46	0.04	2MASS	11.93	0.05	02nov03	8.231	0.05	04nov03
		11.52	0.02	2MASS
06249-0953	1	13.81*	0.09	10feb04	12.63*	0.06	10feb04	12.469	0.18	02nov03
06249-0953	2	12.457	0.25	02nov03
06297+1021(E)	1	11.15	0.02	2MASS	9.30	0.05	02nov03	7.049	0.05	03nov03
		9.17	0.02	2MASS
06297+1021(E)	2	20.24	0.03	13feb04	>15.47	0.05	02nov03	12.041	0.13	03nov03
		17.17	0.05	13feb04
06297+1021(W)	1	9.35	0.03	2MASS	8.14	0.05	02nov03	6.379	0.05	03nov03
		7.97	0.02	2MASS	6.177	0.05	16nov05
06381+1039	1	16.73	0.19	11feb04	14.33	0.17	02nov03	12.573	0.06	03nov03
06382+0939	1	11.07	0.04	13feb04	8.70	0.05	13feb04	6.591	0.05	03nov03
06382+0939	2	11.11	0.04	13feb04	9.76	0.05	13feb04	9.049	0.05	03nov03
06382+0939	3	14.25	0.04	13feb04	12.88	0.06	13feb04	12.508	0.08	03nov03
06382+1017	1a	15.71*	0.03	11feb04	12.83*	0.19	11feb04	9.031*	0.07	02nov03
		9.300	0.05	15nov05
06382+1017	1b	11.371	0.05	15nov05
06382+1017	2	>19.93	0.03	11feb04	14.45	0.05	11feb04	11.609	0.05	02nov03
		11.433	0.06	15nov05
06382+1017	3	>20.48	0.03	11feb04	15.30	0.05	11feb04	11.747	0.06	02nov03
06393+0913	1	12.01	0.03	13feb04	10.47	0.05	02nov03	9.168	0.07	04nov03
		10.45	0.05	13feb04
06393+0913	2	14.66	0.03	13feb04	13.17	0.06	02nov03	12.122	0.18	04nov03
		13.15	0.05	13feb04
07018-1005(E)	1	12.61	0.04	2MASS	10.80	0.03	2MASS	8.71	0.05	03nov03
07018-1005	2	11.84	0.02	2MASS	10.71	0.03	2MASS	10.05	0.05	03nov03
07018-1005	3	13.08	0.03	2MASS	12.36	0.03	2MASS	11.95	0.11	03nov03
07018-1005(W)	4	11.26	0.07	03nov03
07018-1005	5	13.08	0.14	03nov03
07018-1005	6	13.40	0.04	2MASS	12.63	0.03	2MASS	11.60	0.08	03nov03
07025-1204	1a	11.80*	...	2MASS	11.14*	0.05	2MASS	11.33	0.05	16nov05
07025-1204	1b	11.80*	...	2MASS	11.14*	0.05	2MASS	11.38	0.05	16nov05
07025-1204(S)	2	13.53	...	2MASS	11.60	...	2MASS	9.67	0.08	16nov05
07025-1204	3	17.10	...	2MASS	13.74	...	2MASS	11.28	0.06	16nov05
07025-1204(N)	4a	12.65	...	2MASS	10.82	...	2MASS	8.94	0.06	16nov05
07025-1204	4b	13.45	0.05	16nov05
07025-1204	5	13.94	...	2MASS	13.06	...	2MASS	12.53	0.09	16nov05
07025-1204	6	9.96	0.05	16nov05
07025-1204	7	14.86	...	2MASS	13.78	...	2MASS	13.40	...	16nov05
07025-1204	8	15.24	...	2MASS	14.05	...	2MASS	14.01	...	16nov05
07028-1100		16.29	0.03	11feb04	13.18	0.05	11feb04	8.30	...	17nov04
07180-2356		14.36	0.09	11feb04	11.86	0.08	11feb04
07334-2320		16.64	0.21	12feb04	14.37	0.22	11feb04
08043-3343(N)	1	15.35	0.13	2MASS	12.93	0.04	2MASS	11.38	0.06	16nov05

Table 4—Continued

IRAS	# ^a	H	δH^b	date	K	δK^b	date	L'	$\delta L'^b$	date
08043-3343	2	13.01	0.21	16nov05
08043-3343(S)	3	16.00	0.17	2MASS	13.91	0.05	2MASS	11.44	0.07	16nov05
13547-3944	1	7.69	0.06	19jun04	6.78	0.06	19jun04	5.54	0.05	19jun04
13547-3944	2	9.19	0.54	19jun04	9.17	0.07	19jun04	9.14	0.07	19jun04
15398-3359		15.13	0.03	27may04	13.468	0.05	27may04	10.83	0.05	23may04
15420-4553		13.01	0.21	16nov05
16235-2416	1	7.23	0.03	27may04	6.26	0.05	27may04	5.721	0.05	23may04
16240-2430(E)		11.73	0.08	26may04	7.16	0.07	26may04	3.509	0.06	23may04
		7.42	0.07	28jul04	3.398	0.09	26may04
16240-2430(W)		10.54	0.04	26may04	7.82	0.06	28jul04	5.679	0.06	23may04
		5.797	0.05	26may04
16288-2450(E)	1	13.37*	0.04	24may04	10.13*	0.05	24may04	7.300	0.05	18jun04
		7.181	0.10	23may04
16288-2450(E)	2	13.37*	0.03	24may04	10.13*	0.05	24may04	9.468	0.09	18jun04
		9.772	0.05	23may04
16288-2450(W)	1	9.68	0.03	28jul04	7.85	0.05	28jul04	6.024	0.05	01aug04
		5.837	0.11	23may04
16288-2450(W)	2	10.05	0.03	28jul04	8.69	0.05	28jul04	7.760	0.05	01aug04
		7.773	0.12	23may04
16288-2450(W)	3	14.93	0.05	28jul04	12.86	0.06	28jul04	12.324	0.08	01aug04
		11.874	0.05	23may04
16289-4449		8.64	0.07	28may04	7.21	0.08	28may04	4.982	0.06	28may04
16295-4452		15.38	0.12	27may04	12.35	0.08	27may04	9.320	0.05	27may04
16316-1540		9.58	0.04	24may04	8.28	0.05	24may04	6.316	0.08	23may04
16442-0930		13.05	0.07	26may04	8.787	0.07	23may04
		12.77	0.05	2MASS	10.92	0.03	2MASS
16544-1604		17.24	0.05	27may04	13.97	0.07	24may04	12.149	0.12	24may04
		14.06	0.06	27may04
17364-1946	1	16.61	0.12	27may04	13.61	0.09	27may04	10.25	0.16	18jun04
		10.28	0.05	27may04
17369-1945	1	16.49	0.14	24may04	13.71	0.10	24may04	10.09	0.07	23may04
17369-1945	2	15.63	0.08	24may04	13.65	0.05	24may04	11.05	0.08	23may04
17369-1945	3	17.08	0.18	24may04	15.20	0.12	24may04	13.13	0.05	23may04
17369-1945	4	15.41	0.05	24may04	13.56	0.05	24may04	11.92	0.05	23may04
17369-1945	5	17.35	0.18	24may04	15.16	0.08	24may04	13.83	0.05	23may04
17369-1945	6	16.39	0.05	24may04	13.69	0.05	24may04	11.41	0.05	23may04
17441-0433	1	15.58	0.25	26may04	12.93	0.06	26may04	10.19	0.09	19jun04
		10.83	0.05	26may04
18250-0351		4.32	0.12	18jun04
18264-0143		10.34	0.16	23may04
18270-0153(W)	1	11.72	0.04	26may04	10.14	0.05	26may04	8.08	0.05	23may04
18270-0153	2	>19.24	...	26may04	16.38	0.05	26may04	12.38	0.08	23may04
18270-0153	3	19.70	...	26may04	15.41	0.05	26may04	10.66	0.06	23may04
18270-0153	4	18.50	...	26may04	13.32*	0.24	26may04	9.90	0.08	23may04
18270-0153	5	>19.24	...	26may04	13.32*	0.24	26may04	12.13	0.05	23may04
18270-0153(E)	6	14.08	0.08	26may04	11.89	0.07	26may04	9.95	0.07	23may04

Table 4—Continued

IRAS	# ^a	H	δH^b	date	K	δK^b	date	L'	$\delta L'^b$	date
18270-0153	7	>19.24	...	26may04	14.96	0.05	26may04	11.26	0.05	23may04
18273+0034	3	18.27	...	2MASS	15.62	...	2MASS	14.22	0.05	23may04
18273+0034	4	16.41	...	2MASS	14.54	...	2MASS	12.61	0.05	23may04
18274-0212		15.81	0.04	26may04	11.66	0.06	26may04	6.93	0.05	19jun04
		7.05	0.05	26may04
18275+0040		8.60	0.03	26may04	7.72	0.06	26may04	6.17	0.06	23may04
18278-0212	1	14.98	0.04	26may04	11.24	0.05	26may04	8.16	0.05	23may04
18278-0212	2	16.34	0.06	26may04	11.81	0.05	26may04	8.31	0.05	23may04
18318-0434	1	12.23	0.08	28may04	10.77	0.07	28may04	9.83	0.06	28may04
18318-0434	2	13.98	0.12	28may04	12.87	0.09	28may04	12.24	0.05	28may04
18318-0434	3	13.22	0.08	28may04	12.13	0.07	28may04	11.71	0.07	28may04
18318-0434	4	13.06	0.08	28may04	11.99	0.07	28may04	11.50	0.09	28may04
18339-0224	1	12.81	0.04	27may04	12.70	0.05	27may04	12.36	0.08	27may04
18339-0224	2	14.44	0.04	27may04	13.29	0.05	27may04	12.07	0.04	27may04
18340-0116	1	16.85	0.04	26may04	13.20	0.06	26may04	10.48	0.05	23may04
		10.82	0.05	26may04
18340-0116	2	>20.70	...	26may04	15.16	0.08	26may04	11.42	0.15	23may04
		11.86	0.18	26may04
18340-0116	3	>20.70	...	26may04	16.95	0.06	26may04	11.86	0.07	23may04
		12.16	0.06	26may04
18341-0113	1	10.76	0.03	26may04	9.80	0.05	26may04	8.37	0.05	23may04
18341-0113	2	12.83	0.23	26may04	10.86	0.21	26may04	9.84	0.07	23may04
18341-0113	3	>18.27	...	26may04	14.32	0.06	26may04	11.89	0.14	23may04
18383+0059	1	12.01*	0.04	26may04	9.80*	0.05	26may04	8.03	0.05	18jun04
		7.95	0.05	23may04
18383+0059	2	12.01*	0.04	26may04	9.80*	0.05	26may04	9.64	0.07	18jun04
		9.48	0.06	23may04
18383+0059	3	14.04	0.07	26may04	10.91	0.05	26may04	7.68	0.04	18jun04
		7.54	0.05	23may04
18383+0059	4	14.30	0.06	26may04	12.78	0.06	26may04	11.84	0.08	18jun04
		11.86	0.06	23may04
18558+0041	3	15.75	0.04	26may04	13.21	0.05	26may04	11.51	0.12	26may04
18558+0041	4	14.05	0.04	26may04	12.65	0.05	26may04	12.58	0.07	26may04
18558+0041	5	16.08	0.04	26may04	13.97	0.05	26may04	13.73	0.15	26may04
18558+0041	6	14.99	0.04	26may04	13.36	0.10	26may04	13.53	0.05	26may04
18585-3701(E)	1	5.11	0.05	18jun04
18585-3701(W)	1
19247+2238	1	10.78	0.05	26may04	9.84	0.05	26may04	8.37	0.05	23may04
19247+2238	2	10.64	0.04	26may04	10.07	0.05	26may04	9.07	0.05	23may04
19247+2238	3	11.27*	0.04	26may04	10.69*	0.05	26may04	10.40	0.07	23may04
19247+2238	4	11.27*	0.03	26may04	10.69*	0.05	26may04	11.50	0.06	23may04
19247+2238	5	14.04	0.04	26may04	13.55	0.09	26may04	13.33	0.05	23may04
19266+0932		10.26	0.08	26may04	9.68	0.07	26may04	8.17	0.05	23may04
19411+2306	1	11.65*	0.06	03nov03	9.57*	0.08	18jun04	7.73	0.07	04nov03
		8.09	0.06	23may04
19411+2306	2	11.65*	0.06	03nov03	9.57*	0.08	18jun04	8.02	0.10	04nov03

Table 4—Continued

IRAS	# ^a	H	δH^b	date	K	δK^b	date	L'	$\delta L'^b$	date
		8.50	0.08	23may04
19411+2306	3	14.59	0.12	03nov03	12.06	0.06	...	9.95	0.04	04nov03
		14.31	0.12	18jun04	10.35	0.06	23may04
19411+2306	4	14.96	0.21	18jun04	14.27	0.25	18jun04	10.88	0.07	04nov03
		11.33	0.05	23may04
19411+2306	5	14.85	0.07	03nov03	12.92	0.10	18jun04	11.06	0.15	04nov03
		14.80	0.04	18jun04	11.50	0.04	23may04
19411+2306	6	14.81	0.08	03nov03	14.14	0.24	18jun04	14.30	0.04	04nov03
		14.71	0.05	18jun04	14.96	0.04	23may04
19411+2306	7	16.55	0.10	03nov03	14.75	0.07	18jun04	13.67	0.04	04nov03
		15.95	0.04	18jun04	13.77	0.04	23may04
19411+2306	8	15.06	0.07	03nov03	14.17	0.10	18jun04	13.28	0.04	04nov03
		14.99	0.04	18jun04	13.80	0.04	23may04
20355+6343		11.94	0.04	26may04	10.40	0.05	26may04	8.40	0.11	26may04
20377+5658		11.10	0.03	03nov03	9.48	0.05	01nov03	7.08	0.05	02nov03
		7.34	0.06	18jun04
20453+6746		8.57	0.04	28jul04	6.47	0.05	26may04	6.68	0.05	01aug04
		6.53	0.06	28jul04	4.55	0.05	26may04
20568+5217		9.63	0.04	03nov03	7.90	0.05	01nov03	4.87	0.04	02nov03
		4.80	0.05	16nov05
20582+7724		10.37	0.04	28jul04	8.94	0.06	28jul04	7.34	0.05	16nov05
21004+7811	1	8.09	0.04	28jul04	6.26	0.05	28jul04	7.16	0.04	01aug04
21004+7811	2	9.920	0.03	28jul04	8.78	0.05	28jul04	9.62	0.05	01aug04
21007+4951	1	>17.20	0.03	03nov03	13.15	0.10	01nov03	8.09	0.05	02nov03
		15.18	0.03	19jun04	8.46	0.06	18jun04
21007+4951	2	11.47	0.03	03nov03	10.40	0.05	01nov03	8.52	0.04	02nov03
		11.22	0.09	19jun04	8.63	0.05	18jun04
21017+6742(E)	1	12.01	0.04	27may04	10.22	0.05	27may04	8.67	0.06	27may04
21017+6742(W)	1	18.93	0.04	27may04	14.49	0.06	27may04
21025+5221	1	>19.61	0.03	03nov03	13.48	0.05	01nov03	9.14	0.05	01nov03
		19.73	0.04	18jun04	13.62	0.08	18jun04	9.00	0.05	18jun04
21025+5221	2	16.30	0.04	03nov03	12.85	0.05	01nov03	10.60	0.04	01nov03
		16.02	0.06	18jun04	12.73	0.08	18jun04	10.39	0.04	18jun04
21025+5221	3	17.56	0.06	03nov03	13.65	0.05	01nov03	11.48	0.07	01nov03
		17.57	0.06	18jun04	13.79	0.08	18jun04	11.36	0.05	18jun04
21025+5221	4	17.39	0.07	03nov03	13.78	0.05	01nov03	10.72	0.07	01nov03
		17.48	0.04	18jun04	13.78	0.07	18jun04	10.71	0.04	18jun04
21025+6801		12.67	0.03	28may04	11.69	0.05	28may04	11.41	0.07	28may04
21169+6804	1	8.94	0.07	01aug04
		9.14	0.11	26may04
21169+6804	2	16.20	...	26may04	14.59	0.05	26may04	14.06	0.04	01aug04
21169+6804	3	16.13	...	26may04	14.56	0.05	26may04	13.86	0.20	01aug04
21352+4307		14.37	0.04	03nov03	11.75	0.05	01nov03	7.85	0.04	02nov03
		7.75	0.04	18jun04
21388+5622	1	13.94	0.05	03nov03	12.13	0.09	01nov03	9.67	0.06	03nov03
		10.22	0.07	16nov05

Table 4—Continued

IRAS	# ^a	H	δH^b	date	K	δK^b	date	L'	$\delta L'^b$	date
21388+5622	2a	~19.04	...	03nov03	14.29	0.30	01nov03	11.00	0.21	03nov03
		10.72	0.07	16nov05
21388+5622	2b	~19.04	...	03nov03	14.29	0.30	01nov03	11.10	0.22	03nov03
		10.39	0.09	16nov05
21388+5622	3	13.62	0.05	03nov03	12.47	0.06	01nov03	11.05	0.10	03nov03
		11.00	0.06	16nov05
21388+5622	4	14.40	0.09	03nov03	13.49	0.13	01nov03	12.34	0.10	03nov03
		12.23	0.10	16nov05
21388+5622	12	12.68	0.03	03nov03	12.07	...	01nov03	11.61	0.11	03nov03
		11.23	0.05	16nov05
21388+5622	13	14.62	0.06	03nov03	13.68	...	01nov03	12.43	0.18	03nov03
		12.81	0.06	16nov05
21391+5802		>19.00	0.04	04nov03	10.23	0.23	03nov03
		10.85	0.19	19jun04
21432+4719	1a	12.72	0.04	04nov03	11.57	0.09	04nov03	11.75	...	04nov03
21432+4719	1b	11.98	...	04nov03
21432+4719	1c	12.56	...	04nov03
21445+5712	1	11.81	0.08	03nov03	10.25	0.13	01nov03	7.69	0.11	01nov03
		7.67	0.06	27may04
21454+4718	1	8.23	0.03	28may04	7.03	0.05	28may04	5.57	0.05	16nov05
		5.74	0.07	23may04
21569+5842	1	12.79	0.25	04nov03	10.25	0.07	04nov03	7.49	0.05	02nov03
		7.52	0.05	18jun04
		7.52	0.04	19jun04
22051+5848	1	13.02	0.03	03nov03	11.23	0.20	04nov03	9.19	0.04	02nov03
22176+6303	1	1.67	0.06	16nov05
22176+6303	2a	4.58	0.05	16nov05
22176+6303	2b	6.34	0.06	16nov05
22266+6845	1	12.05*	0.03	26may04	10.49*	0.05	26may04	8.36	0.05	16nov05
		11.68	0.04	28jul04	8.42	0.08	26may04
22266+6845	2	20.19	...	26may04	15.02	0.06	26may04	10.39	0.05	16nov05
		16.38	0.04	28jul04	10.72	0.08	26may04
22266+6845	3	10.50	0.05	16nov05
		10.18	0.09	26may04
22272+6358E	1	10.58	0.04	28may04	8.18	0.05	28may04	5.89	0.04	28may04
22272+6358E	2	14.45	0.04	28may04	13.03	0.05	28may04	10.99	0.06	28may04
22272+6358W		16.37	0.05	28may04	13.70	0.05	28may04	11.17	0.06	28may04
F22324+4024		10.68	0.15	29dec04	9.46	0.10	29dec04	6.17	0.05	23may04
22376+7455	1a	15.87	0.18	28jul04	13.34	0.14	28jul04	9.55	0.05	01aug04
		9.69	0.07	16nov05
22376+7455	1b	12.10	0.06	16nov05
22376+7455	2	13.72	0.05	28jul04	12.89	0.07	28jul04	11.77	0.08	01aug04
		11.70	0.08	16nov05
22376+7455	3	13.78	0.05	28jul04	12.89	0.07	28jul04	12.29	0.13	01aug04
		12.06	0.09	16nov05
22376+7455	4	11.27	0.06	28jul04	10.99	0.07	28jul04	11.30	0.08	01aug04

Table 4—Continued

IRAS	# ^a	H	δH^b	date	K	δK^b	date	L'	$\delta L'^b$	date
		10.93	0.07	16nov05
22376+7455	5	13.47	0.07	28jul04	13.05	0.05	28jul04	12.16	0.15	01aug04
		11.75	0.11	16nov05
22376+7455	6	17.893	0.03	28jul04	15.09	0.05	28jul04	13.00	0.16	01aug04
		13.20	0.07	16nov05
22376+7455	7	>21.369	0.03	28jul04	13.74	0.19	28jul04	12.86	0.28	01aug04
		12.93	0.35	16nov05
22451+6154	1	16.72	0.06	26may04	11.96	0.05	26may04	8.11	0.05	26may04
22451+6154	2	12.35	0.04	26may04	10.74	0.05	26may04	9.70	0.05	26may04
22451+6154	3	16.37	0.04	26may04	14.15	0.05	26may04	12.44	0.05	26may04
22451+6154	5	16.50	0.05	26may04	14.29	0.05	26may04	12.23	0.05	26may04
22517+6215	1	15.86	0.03	28may04	13.30	0.05	28may04	11.38	0.04	28may04
22517+6215	2	>19.71	0.03	28may04	17.62	0.05	28may04	11.80	0.06	28may04
22517+6215	3	>19.71	0.03	28may04	17.73	0.05	28may04	12.48	0.09	28may04
22517+6215	4	>19.71	0.03	28may04	15.08	0.05	28may04	11.99	0.09	28may04
22517+6215	5	13.53	0.04	28may04	12.99	0.05	28may04	12.79	0.06	28may04
23037+6213(E)	1
23037+6213	2
23037+6213	3
23037+6213(W)	4
F23591+4748	1	11.65	0.04	03nov03	10.42	0.05	02nov03	9.26	0.04	03nov03
F23591+4748	2	13.79	0.04	03nov03	12.10	0.05	02nov03	10.20	0.04	03nov03
F23591+4748	3	12.43	0.03	03nov03	12.11	0.05	02nov03	12.30	0.07	03nov03

^aThe identifier of the L' source in the finder chart

^bThe photometric uncertainty in this filter, as described in section 3.5

Note. — *: Photometry includes flux from this source and an adjacent source, which were not resolved in this wavelength

Table 5. Binary Properties

IRAS	# ^a	d (pc)	ΔL^b	r (") ^c	PA ^d	Discoverer
03220+3035		290	1.30	1.37	200.3	Hodapp (1994)
F03258+3105		220	0.05	0.99	91.5	new
03260+3111	1	290	0.81	0.55	81.7	new
03260+3111	1	290	3.29	3.77	49.2	Haisch et al. (2004)
03331+6256	1	1560	0.05	2.34	212.4	new
04073+3800	1	350	5.18	12.94	28.6	Weintraub (1992)
04108+2803	2	140	0.44	21.64	64.5	Myers et al. (1987)
04113+2758	1	140	0.60	3.97	154.3	Kenyon et al. (1990)
04169+2702	1	140	1.63	0.18	106.6	new
04189+2650	1	140	2.99	0.31	128.9	new
04189+2650	2	140	2.84	19.75	275.7	Mundt et al. (1984)
04191+1523		140	3.27	5.97	305.2	Duchêne et al. (2004)
04223+3700		350	3.56	1.10	85.6	new
04239+2436		140	1.47	0.30	282.7	Reipurth et al. (2000)
04288+2417		140	3.50	2.30	171.4	Cohen & Kuhi (1979)
04325+2402		140	2.63	8.03	351.4	Hartmann et al. (1999)
05155+0707	1	460	2.78	6.58	73.4	Osterloh et al. (1997)
05283–0412	1	470	0.47	4.54	308.8	new
05289–0430 E		470	2.64	0.29	346.2	new
05302–0537		470	0.16	0.65	27.4	new
05327–0457	1	450	1.23	0.14	80.3	new
05327–0457	2	450	0.49	2.25	237.1	new
05327–0457	6	450	0.50	3.63	184.7	new
05327–0457	5	450	0.31	2.77	335.4	new
05340–0603	2	470	0.78	0.24	357.3	new
05375–0040	1	470	1.68	6.40	279.0	new
05379–0758	1	480	4.11	0.52	0.7	new
05384–0807	1	480	1.81	0.37	141.5	new
05384–0807	3	480	1.89	0.18	355.3	new
05384–0807	4	480	0.78	0.08	327.5	new
05384–0807	6	480	0.73	0.16	314.4	new
05391–0841	1	480	3.76	0.72	311.7	new
05391–0841	2	480	3.28	5.38	164.3	Chen & Tokunaga (1994)
			0.45	9.49	333.8	Chen & Tokunaga (1994)
05404–0948		480	2.49	3.59	204.9	new
05404–0948		480	2.36	0.16	135.3	new
05417+0907		465	0.86	1.21	209.7	new
05427–0116		470	1.32	0.81	351.6	new
05548–0935	2	470	0.87	4.22	22.9	new
05548–0935	2	470	0.37	10.55	222.5	new
05555–1405	1	470	0.08	5.80	177.6	new
05555–1405	1	470	1.55	0.21	115.2	new
05564–1329		470	0.68	4.48	252.0	new
05598–0906	1	470	4.23	0.93	98.8	new
05598–0906	5	470	0.90	0.44	177.8	new
05598–0906	7	470	3.45	0.85	15.3	new

Table 5—Continued

IRAS	# ^a	d (pc)	$\Delta L'$ ^b	r (") ^c	PA ^d	Discoverer
06249–0953		830	0.33	2.30	262.6	new
06297+1021 E		830	4.94	5.50	341.8	new
06382+1017	1	800	2.46	1.82	336.6	Piché et al. (1995)
06382+1017	1	800	1.85	0.21	16.1	new
07025–1204	2	1150	0.43	0.34	330.4	new
07025–1204	2	1150	1.56	2.37	142.7	new
07025–1204	4	1150	3.58	1.49	356.6	new
07025–1204	4	1150	4.45	0.62	355.8	new
07028–1100	1	1150	3.94	2.37	48.1	new
16288–2450 E		160	2.85	0.62	199.8	new
16288–2450 W		160	1.95	2.98	241.0	Hodapp (1994)
16288–2450 W		160	5.88	14.72	127.4	new
17369–1945	1	160	0.96	1.50	78.4	new
17369–1945	1	160	2.68	1.59	30.5	new
17369–1945	1	160	1.83	3.48	356.6	new
18270–0153	1	none	4.21	5.68	63.7	new
18270–0153	4	none	2.19	1.48	70.6	new
18270–0153	6	none	1.25	1.93	313.8	new
18273+0034	2	310	2.51	9.53	302.8	new
18278–0212	1	600	0.15	4.47	328.0	new
18340–0116	1	none	1.47	2.83	32.3	new
18340–0116	1	none	1.43	7.90	36.8	new
18383+0059	3	none	0.39	2.15	280.8	new
18383+0059	1	none	1.85	0.18	141.3	new
19247+2238	1	none	0.69	1.57	143.7	new
19247+2238	3	none	0.97	0.24	6.3	new
21004+7811		300	2.52	2.47	235.3	new
21025+5221	1	none	1.41	4.72	35.7	new
21025+5221	3	none	0.50	3.47	324.3	new
21169+6804	1	450	4.10	8.97	92.0	Yun & Clemens (1994)
21169+6804	3	450	0.32	1.01	68.5	new
21388+5622	2	750	0.63	0.71	133.2	new
21388+5622	3	750	1.34	2.49	47.6	new
21432+4719	1	900	0.04	0.66	119.5	new
21432+4719	1	900	1.17	1.52	13.3	new
22266+6845	1	200	2.18	6.95	292.2	new
22266+6845	1	200	2.16	0.62	10.0	new
22272+6358E	1	950	5.08	6.19	330.2	new
22376+7455	1	330	2.22	0.54	176.3	new
22376+7455	2	330	0.49	0.49	340.0	new
22376+7455	6	330	0.16	1.24	142.6	new
23037+6213	3	700	1.87	4.83	75.5	new
23591+4748		800	0.93	0.98	96.7	new

^aThe number of the primary star in the finder charts if there is more than one primary object per IRAS source.

^bThe L' magnitude difference between the primary and secondary stars.

^cThe angular separation from the primary to the secondary star.

^dThe position angle of the secondary star.

Table 6. Binary Detection Limits

IRAS	# ^c	d (pc)	Inner Detection Limits (") ^a				Outer Detection Limits (") ^b			
			$\Delta L' = 1$	$\Delta L' = 2$	$\Delta L' = 3$	$\Delta L' = 4$	$\Delta L' = 1$	$\Delta L' = 2$	$\Delta L' = 3$	$\Delta L' = 4$
00465+5028		800	0.25	0.30	0.72	999.	6.25	6.25	6.25	6.25
01166+6635		249	0.26	0.26	0.41	0.70	10.53	6.75	5.35	5.05
02086+7600		180	0.39	999.	999.	999.	27.78	20.19	16.01	15.13
03220+3035		290	0.28	0.30	0.42	0.72	17.24	17.24	17.24	17.24
03225+3034		290	0.27	999.	999.	999.	17.24	17.24	17.24	17.24
F03258+3105		220	0.27	0.27	0.27	999.	22.73	22.73	22.73	20.53
03260+3111	1	290	0.30	0.33	0.72	0.96	17.24	17.24	17.24	17.24
03260+3111	10	290	0.27	0.48	0.66	0.84	17.24	17.24	17.24	17.24
03271+3013		290	0.30	999.	999.	999.	17.24	17.24	17.24	17.24
03301+3111		350	0.36	0.60	0.84	1.08	14.29	14.29	14.29	14.29
03301+3057		350	0.50	0.50	999.	999.	14.29	14.29	14.29	14.29
03331+6256	1	1560	0.27	0.37	0.70	999.	3.21	3.21	3.21	3.21
03445+3242		280	0.29	0.29	0.36	0.72	17.86	17.86	17.86	17.86
03507+3801		350	0.25	0.25	0.42	0.66	14.29	14.29	14.29	14.29
04016+2610	1	140	0.25	0.36	0.54	0.78	25.00	25.00	25.00	25.00
04067+3954	1	350	0.36	1.08	999.	999.	14.29	14.29	14.29	14.29
04073+3800	1	350	0.27	0.30	0.36	0.60	14.29	14.29	14.29	14.29
04108+2803	1	140	0.27	0.27	0.90	0.90	25.00	25.00	25.00	22.71
04108+2803	2	140	0.27	0.27	0.90	0.90	25.00	25.00	25.00	22.71
04113+2758	1	140	0.24	0.24	0.30	0.42	25.00	25.00	25.00	25.00
04169+2702	1	140	0.26	0.36	0.48	0.72	25.00	25.00	25.00	25.00
04181+2655	1	140	0.27	0.36	0.60	0.96	25.00	25.00	25.00	25.00
04181+2655	2	140	0.27	0.27	0.42	1.08	25.00	25.00	25.00	25.00
04181+2655	3	140	0.30	0.48	0.60	1.08	25.00	25.00	25.00	25.00
04189+2650	1	140	0.21	0.24	0.42	999.	25.00	25.00	25.00	20.54
04189+2650	2	140	0.20	0.24	0.55	0.67	25.00	25.00	25.00	25.00
04191+1523		140	0.27	0.48	0.72	1.20	25.00	25.00	25.00	20.54
04223+3700		350	0.26	0.26	0.42	0.72	14.29	14.29	14.29	14.29
04239+2436		140	0.32	0.60	0.72	1.08	25.00	25.00	25.00	25.00
04240+2559	1	140	0.09	0.09	0.21	0.34	25.00	25.00	25.00	25.00
04248+2612	1	140	0.24	0.36	0.48	999.	25.00	25.00	25.00	25.00
04275+3531		350	0.25	999.	999.	999.	14.29	14.29	14.29	14.29
04287+1801 E		140	0.60	0.96	1.02	1.38	25.00	25.00	25.00	25.00
04288+2417		140	0.31	0.32	0.75	1.17	25.00	25.00	25.00	25.00
04292+2422	1	140	0.26	0.30	0.24	0.42	25.00	25.00	25.00	25.00
04292+2422	2	140	0.26	0.26	0.36	0.60	25.00	25.00	25.00	25.00
04295+2251		140	0.27	0.30	0.42	0.96	25.00	25.00	25.00	24.35
04315+3617		350	0.27	0.30	0.36	0.60	14.29	14.29	14.29	14.29
04325+2402		140	0.36	999.	999.	999.	25.00	25.00	25.00	20.54
04327+5432		170	0.28	0.36	0.54	999.	20.59	20.59	18.70	16.35
04365+2535		140	0.45	0.48	0.78	1.44	25.00	25.00	25.00	25.00
04369+2539		140	0.24	0.36	0.42	0.66	25.00	25.00	25.00	25.00
04381+2540		140	0.61	999.	999.	999.	25.00	25.00	25.00	22.71
04530+5126		170	0.08	0.08	0.15	0.25	25.00	25.00	25.00	25.00
04591–0856		210	0.24	0.36	0.54	0.96	23.81	23.81	23.81	22.71

Table 6—Continued

IRAS	# ^c	d (pc)	Inner Detection Limits (″) ^a				Outer Detection Limits (″) ^b			
			$\Delta L' = 1$	$\Delta L' = 2$	$\Delta L' = 3$	$\Delta L' = 4$	$\Delta L' = 1$	$\Delta L' = 2$	$\Delta L' = 3$	$\Delta L' = 4$
05155+0707	1	460	0.27	0.48	1.08	999.	10.87	10.87	10.87	10.79
05283–0412	1	470	0.24	0.24	999.	999.	10.64	10.64	10.43	10.08
05286+1203		470	0.30	0.60	999.	999.	10.64	10.64	10.43	10.08
05289–0430 E		470	0.11	0.11	0.24	0.38	10.64	10.64	10.64	10.64
05289–0430 W		470	0.11	0.11	0.26	0.38	10.64	10.64	10.64	10.64
05302–0537		470	0.26	0.26	0.42	0.90	10.64	10.64	10.64	10.64
05311–0631		470	0.24	0.24	0.24	0.36	10.64	10.64	10.64	10.64
05320–0300	1	470	0.20	0.36	0.36	0.66	10.64	10.64	10.64	10.64
05320–0300	2	470	0.20	999.	999.	999.	10.64	10.64	10.64	10.64
05320–0300	3	470	0.20	0.20	999.	999.	10.64	10.64	10.64	10.64
05327–0457 E		450	0.26	0.30	0.48	0.72	11.11	11.11	11.11	11.11
05327–0457	1	450	0.11	0.17	0.30	0.43	11.11	11.11	11.11	11.11
05327–0457	2	450	0.11	999.	999.	999.	11.11	11.11	11.11	11.11
05327–0457	6	450	0.26	999.	999.	999.	11.11	11.11	11.11	11.11
05327–0457	5	450	0.11	0.11	0.21	999.	11.11	11.11	11.11	11.11
05340–0603	1	470	0.28	0.28	0.43	999.	10.64	10.64	10.64	10.43
05340–0603	2	470	0.26	0.75	999.	999.	10.64	10.64	10.64	10.43
05357–0650	1	470	0.10	0.10	0.17	0.30	10.64	10.64	10.64	10.64
05375–0040	1	470	0.10	0.09	0.13	0.30	10.64	10.64	10.64	10.64
05375–0040	3	470	0.09	0.13	0.29	999.	10.64	10.64	10.64	10.64
05378–0750	1	480	0.27	0.30	0.78	999.	10.42	10.42	10.42	10.42
05378–0750	2	480	0.24	0.24	0.30	0.60	10.42	10.42	10.42	10.42
05379–0758	1	480	0.24	0.24	0.54	0.72	10.42	10.42	10.42	10.42
05379–0758	2	480	0.24	0.24	999.	999.	10.42	10.42	10.42	10.42
05379–0758	3	480	0.24	0.24	0.60	999.	10.42	10.42	10.42	10.42
05384–0807	1	480	0.11	0.11	0.17	0.30	10.42	10.42	10.42	10.42
05384–0807	3	480	0.30	0.30	0.48	0.72	10.42	10.42	10.42	10.42
05384–0807	4	480	0.11	0.17	999.	999.	10.42	10.42	10.42	10.42
05384–0807	5	480	0.11	0.17	999.	999.	10.42	10.42	10.42	10.42
05384–0807	6	480	0.09	0.13	0.21	0.38	10.42	10.42	10.42	10.42
05391–0841	1	480	0.23	0.23	0.54	1.08	10.42	10.42	10.42	10.42
05391–0841	2	480	0.23	0.23	0.36	0.90	10.42	10.42	10.42	10.42
05403–0818		480	0.24	0.24	0.24	0.84	10.42	10.42	10.42	10.42
05404–0948		480	0.10	0.10	0.10	0.34	10.42	10.42	10.42	10.42
05405–0117		430	0.41	0.60	1.02	999.	11.63	11.63	11.63	11.63
05417+0907		465	0.27	0.30	0.36	999.	10.75	10.75	10.75	10.75
05427–0116		470	0.23	0.23	0.36	0.90	10.64	10.64	10.64	10.64
05510–1018	1	470	0.25	0.25	999.	999.	10.64	10.64	10.43	10.08
05510–1018	2	470	0.30	999.	999.	999.	10.64	10.64	10.43	10.08
05513–1024		470	0.10	0.10	0.17	0.34	10.64	10.64	10.64	10.64
05548–0935	2	470	0.27	0.27	999.	999.	10.64	10.32	9.97	9.97
05555–1405	1	470	0.11	0.11	0.11	0.17	10.64	10.64	10.64	10.64
05555–1405	4	470	0.11	0.13	0.17	0.30	10.64	10.64	10.64	10.64
05564–1329		470	0.22	0.22	0.55	0.84	10.64	10.64	10.64	10.64
05580–1034		470	0.23	0.23	0.48	999.	10.64	10.64	10.43	10.08

Table 6—Continued

IRAS	# ^c	d (pc)	Inner Detection Limits (″) ^a				Outer Detection Limits (″) ^b			
			$\Delta L' = 1$	$\Delta L' = 2$	$\Delta L' = 3$	$\Delta L' = 4$	$\Delta L' = 1$	$\Delta L' = 2$	$\Delta L' = 3$	$\Delta L' = 4$
05581–1026		470	0.25	999.	999.	999.	10.64	10.32	9.97	9.97
05596–0903		470	0.33	0.96	999.	999.	10.64	10.64	10.43	10.08
05598–0906	1	470	0.24	0.30	0.42	0.72	10.64	10.64	10.64	10.64
05598–0906	3	470	0.24	999.	999.	999.	10.64	10.64	10.64	10.64
05598–0906	4	470	0.24	0.24	0.42	999.	10.64	10.64	10.64	10.64
05598–0906	5	470	0.24	0.30	999.	999.	10.64	10.64	10.64	10.64
05598–0906	7	470	0.24	0.36	0.48	999.	10.64	10.64	10.64	10.64
05598–0906	9	470	0.24	999.	999.	999.	10.64	10.64	10.64	10.64
06027–0714		830	0.37	999.	999.	999.	6.02	6.02	6.02	6.02
06033–0710		830	999.	999.	999.	999.	6.02	6.02	6.02	6.02
06047–1117		500	0.24	0.36	0.42	0.66	10.00	10.00	10.00	10.00
06057–0923		830	999.	999.	999.	999.	6.02	6.02	6.02	6.02
06216–1044		830	0.24	0.24	0.36	0.84	6.02	6.02	6.02	6.02
06249–0953		830	0.28	999.	999.	999.	6.02	6.02	6.02	6.02
06297+1021 E		830	0.24	0.30	0.36	0.66	6.02	6.02	6.02	6.02
06297+1021 W		830	0.17	0.21	0.30	0.60	6.02	6.02	6.02	6.02
06381+1039		960	999.	999.	999.	999.	5.21	5.21	5.21	5.21
06382+1017	1	800	0.10	0.10	0.25	0.43	6.25	6.25	6.25	6.25
06382+1017	3	800	0.26	999.	999.	999.	6.25	6.25	6.25	6.25
06393+0913	1	950	0.23	0.23	0.36	0.90	5.26	5.26	5.26	5.26
07018–1005 E	1	1150	0.24	0.48	0.66	1.14	4.35	4.35	4.35	4.35
07025–1204	2	1150	0.10	0.10	0.10	0.34	4.35	4.35	4.35	4.35
07025–1204	4	1150	0.10	0.10	0.17	0.34	4.35	4.35	4.35	4.35
07028–1100	1	1150	0.32	0.60	0.72	1.68	4.35	4.35	4.35	4.35
07180–2356		1500	0.33	0.48	0.84	1.68	3.33	3.33	3.33	3.33
08043–3343 N		none	0.11	0.21	999.	999.	10.64	10.64	10.64	10.64
08043–3343 S		none	0.11	0.17	999.	999.	10.64	10.64	10.64	10.64
13547–3944		550	0.36	0.60	0.96	1.20	9.10	9.10	9.10	9.10
15398–3359		170	999.	999.	999.	999.	18.70	13.82	12.08	11.68
15420–4553		none					25.00	25.00	25.00	25.00
16235–2416		160	0.26	0.36	0.42	0.66	25.00	25.00	25.00	25.00
16240–2430 E		160	0.96	0.96	1.02	1.44	25.00	25.00	25.00	25.00
16240–2430 W		160	0.96	0.96	1.02	1.26	25.00	25.00	25.00	25.00
16288–2450 E		160	0.27	0.36	0.42	1.02	25.00	25.00	25.00	25.00
16288–2450 W		160	0.55	0.55	0.55	1.50	25.00	25.00	25.00	25.00
16289–4449		700	0.96	1.20	1.92	999.	8.33	8.33	6.28	4.98
16295–4452		600	0.92	999.	999.	999.	25.00	25.00	25.00	25.00
16316–1540		160	0.28	0.30	0.42	0.78	25.00	25.00	18.70	13.82
16442–0930		160	0.24	0.36	0.60	999.	8.41	5.39	4.27	4.04
17364–1946		160	0.42	0.48	0.84	1.32	10.56	6.39	4.73	4.13
17369–1945	1	160	0.22	0.22	0.61	999.	10.56	6.39	4.73	4.13
17441–0433		none	0.24	0.36	0.48	999.	10.64	9.95	7.35	6.43
18250–0351		250	0.24	0.36	0.54	0.66	20.00	20.00	20.00	20.00
18264–0143	1	none	0.33	0.60	1.20	999.	5.55	3.55	2.82	2.66
18270–0153	1	none	0.25	0.30	0.42	0.66	10.64	9.85	6.97	4.21

Table 6—Continued

IRAS	# ^c	d (pc)	Inner Detection Limits (″) ^a				Outer Detection Limits (″) ^b			
			$\Delta L' = 1$	$\Delta L' = 2$	$\Delta L' = 3$	$\Delta L' = 4$	$\Delta L' = 1$	$\Delta L' = 2$	$\Delta L' = 3$	$\Delta L' = 4$
18270–0153	4	none	0.25	0.25	0.42	999.	10.64	9.85	6.97	4.21
18270–0153	6	none	0.25	0.25	0.42	999.	10.64	9.85	6.97	4.21
18273+0034	2	310	0.22	0.22	0.30	999.	8.41	5.38	4.27	4.04
18274–0212	1	none	0.23	0.23	0.42	0.66	10.64	10.64	9.85	6.97
18275+0040	1	310	0.21	0.21	0.36	0.54	16.13	16.13	16.13	14.94
18278–0212	1	600	0.19	0.19	0.24	0.36	8.33	8.33	8.33	6.39
18339–0224		none	999.	999.	999.	999.	2.82	2.66	2.66	2.66
18340–0116	1	none	0.24	0.36	0.60	999.	5.55	3.55	2.82	2.66
18341–0113	1	none	0.22	0.22	0.24	0.60	10.64	7.94	5.55	3.55
18341–0113	2	none	0.36	0.48	0.78	999.	10.64	7.94	5.55	3.55
18383+0059	1	none	0.24	0.24	0.24	0.66	10.64	9.85	6.97	4.21
18558+0041	2	none	0.27	999.	999.	999.	6.97	4.21	3.11	2.72
18558+0041	3	none	0.27	0.47	999.	999.	6.97	4.21	3.11	2.72
18558+0041	6	none	999.	999.	999.	999.	6.97	4.21	3.11	2.72
18585–3701		130	0.22	0.60	0.66	0.78	25.00	25.00	25.00	25.00
19247+2238	1	none	0.11	0.13	0.17	0.23	10.64	7.94	5.55	3.55
19247+2238	3	none	0.13	0.17	0.32	999.	10.64	7.94	5.55	3.55
19266+0932		300	0.24	0.24	0.42	0.78	16.67	15.43	10.91	6.60
20355+6343		450	0.48	0.72	0.96	999.	11.11	11.11	11.11	11.11
20377+5658	1	440	0.31	0.42	0.54	0.78	11.36	11.36	11.36	11.36
20453+6746		500	0.09	0.09	0.21	0.34	10.00	10.00	10.00	10.00
20568+5217	1	1270	0.17	0.26	0.38	0.43	3.94	3.94	3.94	3.94
20582+7724		175	0.25	0.53	0.75	999.	25.00	25.00	25.00	25.00
21004+7811		300	0.51	0.51	0.87	1.16	16.67	16.67	16.67	16.67
21007+4951	1	700	0.30	0.36	0.60	0.90	7.14	7.14	7.14	7.14
21007+4951	2	700	0.29	0.48	0.66	0.84	7.14	7.14	7.14	7.14
21017+6742	1	288	0.33	1.20	999.	999.	17.36	17.36	17.36	17.36
21017+6742 W	1	288	0.81	999.	999.	999.	17.36	17.36	17.36	17.36
21017+6742 W	2	288	0.46	0.46	2.16	999.	17.36	17.36	17.36	17.36
21025+5221	1	none	0.23	0.36	0.72	0.96	10.64	10.64	10.64	8.70
21025+5221	3	none	0.23	0.23	999.	999.	10.64	10.64	10.64	8.70
21025+5221	5	none	0.23	0.23	999.	999.	10.64	10.64	10.64	8.70
21169+6804	1	450	0.87	0.87	0.93	1.28	11.11	11.11	11.11	11.11
21169+6804	2	450	999.	999.	999.	999.	11.11	11.11	11.11	11.11
21352+4307		600	0.24	0.36	0.54	0.72	8.33	8.33	8.33	7.91
21388+5622	1	750	0.13	0.21	1.20	999.	6.67	6.67	6.66	5.28
21388+5622	2	750	0.11	0.11	0.17	0.26	6.67	6.67	6.66	5.28
21388+5622	3	750	0.11	0.11	0.17	999.	6.67	6.67	6.66	5.28
21391+5802		750	0.48	0.72	1.20	999.	6.67	6.66	5.28	4.99
21432+4719	1	900	0.31	999.	999.	999.	5.56	5.56	5.28	4.99
21445+5712		360	0.48	1.20	1.20	999.	13.89	13.89	13.89	10.40
21454+4718		900	0.11	0.13	0.30	0.38	5.56	5.56	5.56	5.56
21569+5842		250	0.28	0.36	0.66	0.84	20.00	20.00	14.90	10.40
22051+5884		750	0.84	0.84	0.84	999.	6.67	6.67	6.67	5.84
22266+6845	1	200	0.30	0.32	0.43	0.58	23.56	14.89	10.40	6.66

Table 6—Continued

IRAS	# ^c	d (pc)	Inner Detection Limits (″) ^a				Outer Detection Limits (″) ^b			
			$\Delta L' = 1$	$\Delta L' = 2$	$\Delta L' = 3$	$\Delta L' = 4$	$\Delta L' = 1$	$\Delta L' = 2$	$\Delta L' = 3$	$\Delta L' = 4$
22272+6358E	1	950	0.61	0.61	0.85	1.19	5.26	5.26	5.26	5.26
22324+4024		880	0.36	0.48	0.72	0.84	5.68	5.68	5.68	5.68
22376+7455	1	330	0.10	0.17	0.30	0.38	15.15	15.15	15.15	15.15
22376+7455	2	330	0.10	0.21	0.99	999.	15.15	15.15	15.15	15.15
22376+7455	6	330	0.10	999.	999.	999.	15.15	15.15	15.15	15.15
23037+6213	1	700	0.58	0.58	0.75	999.	7.14	7.14	7.14	7.14
23037+6213	3	700	0.58	0.58	1.07	999.	7.14	7.14	7.14	7.14
23037+6213	4	700	0.96	999.	999.	999.	7.14	7.14	7.14	7.14
23591+4748		800	0.26	0.42	0.66	1.20	6.25	6.25	6.25	6.25

^aThe closest distance from the primary star that a fake companion star of the stated magnitude difference could be detected. If inner detection limit is 999., then a companion of that contrast cannot be detected at any separation.

^bThe farthest that a binary companion could be accepted. This is limited by our 5000 AU separation limit or the 5% contamination criterion.

^cThe number of the primary star in the finder charts if there is more than one primary object per IRAS source.

REFERENCES

- Burnham, R., *Burnham's Celestial Handbook*, Dover Publications, New York, 1978.
- Chen, H. & Tokunaga, A., 1994, *ApJS*, 90, 149
- Cohen, M. & Kuhi, L., 1979, *ApJS*, 41, 743
- Connelley, M., Reipurth, B., & Tokunaga, A., 2007, *AJ*, 133, 1528
- Connelley, M., Reipurth, B., & Tokunaga, A., 2008, *AJ*, in press
- Correia, S., Zinnecker, H., Ratzka, T., & Sterzik, M., 2006, *A&A*, 459, 909
- Covey, K., Greene, T., Doppmann, G., Lada, C., *AJ*, 131, 512
- Duchêne, G., Bouvier, J., Bontemps, S., André, P., & Motte, F., 2004, *A&A*, 427, 651
- Duchêne, G., Delgado-Donate, E., Haisch, K., Loinard, L., & Rodríguez, L., 2007, in *Protostars and Planets V*, eds B. Reipurth, D. Jewitt, & K. Keil, University of Arizona Press, p.379
- Duquennoy, A. & Mayor, M., 1991, *A&A*, 248, 485
- Ghez, A., Neugebauer, G., Gorham, P., Haniff, C., Kulkarni, S., Matthews, K., Koresko, C., & Beckwith, S., 1991, *AJ*, 102, 2066
- Haisch, Jr., K., Greene, T., Barsony, M., & Stahler, S., 2004, *AJ*, 127, 1747
- Hartmann, L., Calvet, N., Allen, L., Chen, H., Jayawardhana, R., 1999, *AJ*, 118, 1784
- Heintz, W., 1969, *JRASC*, 63, 275
- Hodapp, K., 1994, *ApJS*, 94, 615
- Hodapp, K., Hora, J., Hall, D., et al. 1996, *New Astronomy*, 1, 177
- Kenyon, S., Hartmann, L., Strom, K., & Strom, S., 1990, *AJ*, 99, 869
- Kobayashi, N., Tokunaga, A., Terada, H., et al., 2000, *Proc. SPIE 4008*, eds. M. Iye & A. Moorwood, 1056
- Krisciunas, K., 1987, *PASP*, 99, 887

- Lada, C., 1991, in *The Physics of Star Formation and Early Stellar Evolution*, eds. C. J. Lada & N. D. Kylafis, Kluwer Academic Publishers, p.329
- Larson, R., 2001, in *IAU Symposium 200: The Formation of Binary Stars*, eds. H. Zinnecker & R. Mathieu, Astronomical Society of the Pacific, p.93
- Magnier, E., Volp, A., Laan, K., van den Ancker, M., & Waters, L., 1999, *A&A*, 352, 228
- Mathieu, R., Ghez, A., Jensen, E., & Simon, M., 2000, in *Protostars and Planets IV*, eds. Mannings, Boss, & Russell, University of Arizona Press, p.703
- Mathis, J., 2000, in *Allen's Astrophysical Quantities*, ed. Cox, AIP Press
- Meyer, M., Calvet, N., Hillenbrand, L., 1997, *AJ*, 114, 288
- Mitchell, J., 1767, *Roy. Soc. Phil. Trans.*, 57, 234
- Monet, D., Levine, S., Canzian, B., et al., 2003, *AJ*, 125, 984
- Mundt, R., Büehrke, T., Fried, J., Neckel, T., Sarcander, M., Stocke, J., 1984, *A&A*, 140, 17
- Murakawa, K., Suto, H., Tamura, M., et al., 2004, *PASJ*, 56, 509
- Myers, P., Fuller, G., Mathieu, R., Beichman, C., Benson, P., Schild, R., & Emerson, J., *ApJ*, 319, 340
- Osterloh, M., Henning, Th., & Launhardt, R., 1997, *ApJS*, 110, 71
- Patience, J., Ghez, A., Reid, I., & Matthews, K., 2002, *AJ*, 123, 1570
- Piché, F., Howard, E., Pipher, J., 1995, *MNRAS*, 275, 711
- Price, S., Egan, M., Carey, S., Mizuno, D., & Kuchar, T., 2001, *AJ*, 121, 2819
- Ramsay Howat, S., Todd, S., Leggett, S., et al., 2004, *SPIE*, 5492, 1160
- Rayner, J., Toomey, D., Onaka, P., Denault, A., Stahlberger, W., Vacca, W., Cushing, M., Wang, S., 2003, *PASP*, 115, 362
- Reipurth, B., Yu, K., Heathcote, S., Bally, J., & Rodríguez, L., 2000, *AJ*, 120, 1449
- Reipurth, B. & Zinnecker, H., 1993, *A&A*, 278, 81
- Ressler, M. & Shure, M., 1991, *AJ*, 102, 1398

Simons, D. & Tokunaga, A., 2002, PASP, 114, 169

Tokunaga, A. & Simons, D., 2002, PASP, 114, 180

Tokunaga, A., Kobayashi, N., Bell, J., et al., 1998, SPIE, 3354, 512

Weintraub, D., 1992, BAAS, 24, 1141

Yun, J. & Clemens, D., 1994, ApJS, 92, 145

Zinnecker, H., & Wilking, B., 1992, in Binaries as Tracers of Stellar Formation, eds. A. Duquennoy & M. Mayor, Cambridge University Press, p.269